

Chapter 2

Full-Duplex Wireless-Powered Communications

Mohammadali Mohammadi, Batu K. Chalise, and Himal A. Suraweera

2.1 Introduction

Wireless communications have seen a rapid progress since the invention of the radio around the turn of the twentieth century by Guglielmo Marconi. Proliferation of wireless applications, smart phones, and devices has profoundly impacted the everyday lives of people. In most communication systems, radio terminals have a dual role as transmitters and receivers. Such role has been traditionally carried out by employing half-duplex (HD) operation, meaning that the radio terminals transmit and receive in orthogonal time or frequency channels. However, this requires additional spectrum which, in fact, is scarce. In their quest to find a solution for this spectrum scarcity problem, academic and industrial communities have focused on full-duplex (FD) communications, where the terminals are allowed to transmit and receive simultaneously over the same frequency band [1, 2].

The history of FD wireless dates back to around 1940s when the principle was mainly used in radar systems [1]. However, until very recently, FD was not considered to be feasible due to the effects of self-interference (SI). This view has been radically changed since prototypes and efficient SI cancellation algorithms

M. Mohammadi (✉)

Faculty of Engineering, Shahrekord University, Shahrekord 115, Iran
e-mail: m.a.mohammadi@eng.sku.ac.ir

B.K. Chalise

Department of Electrical Engineering and Computer Science, Cleveland State University,
Cleveland, OH 44115-2214, USA
e-mail: batu.k.chalise@ieee.org

H.A. Suraweera

Department of Electrical and Electronic Engineering, University of Peradeniya,
Peradeniya 20400, Sri Lanka
e-mail: himal@ee.pdn.ac.lk

have emerged through the development of electronics and antenna theory [3–5]. In FD systems, the significant power difference between the transmitted signal and the received signal causes SI. Such strong SI can saturate the front end of the receiver to cause severe performance degradation [6–8].

Present methods to mitigate SI in FD transceivers can be classified into two broad categories as: analog and digital SI cancellation techniques [4]. Further, analog domain SI cancellation techniques can be subdivided into passive suppression techniques and active analog techniques. Examples of former include the placement of a radio frequency (RF) absorber to block the path between the transmitter and receiver, polarization and the deployment of directional antennas [9]. These methods rely on propagation path loss for attenuation of the transmitted signal at the receiver. On the other hand, active analog cancellation techniques rely on methods such as specific antenna placement and the use of delay lines to cancel the RF analog signal. Other options for SI cancellation exist in the digital domain, where with the help of reference signals and adaptive filtering, SI can be estimated and removed. Often a combination of both analog and digital cancellation methods are required to reduce the SI up to tolerable levels and to make FD operation practical [10]. Nevertheless, perfect SI cancellation is not possible due to nonlinear distortion caused by transmitter and receiver imperfections [7].

The use of FD has already been advocated for small cells, wireless local area networks (WLANs), and fifth generation (5G) systems [1, 2, 8, 11]. In addition, applications of FD technology in cognitive radio systems [12] and physical layer security [13] have also been considered. For example, simultaneous sensing and data transmission function allowed by FD radios can improve the sensing performance and secondary throughput in cognitive radio systems. Transmission of artificial noise to interfere the eavesdropper is an effective technique used for improving the wireless security. To this end, FD radios allow simultaneous transmission of jamming signals and reception of useful signals and hence become a natural solution to improve the secrecy.

2.1.1 Wireless-Powered Communications

Emergence of multi-media rich wireless applications has created a high demand for energy. Terminals in contemporary wireless networks are either connected to the electrical grid or rely on batteries for operation. Therefore, limited operational lifetime of such wireless terminals imposes strict constraints on the network performance. In this context, energy harvesting communications have emerged as a viable solution to supply power to wireless devices by letting them scavenge energy from resources such as photovoltaic, wind, vibrational, thermoelectric, and RF signals [14]. Already, tremendous research progress has been achieved to bring energy harvesting from an interesting theoretical concept to a technological maturity [15–17].

Energy harvesting from solar, wind, etc. present significant challenges due to the intermittent nature of these sources [14]. An alternative reliable source of energy that can overcome this issue is offered by ambient and directed RF signals. It is well accepted that RF sources can provide a controllable energy flow to replenish the depleted energy supply of wireless nodes and sensors [18]. However, to realize such wireless-powered communication systems, several key design aspects are yet to be comprehensively investigated. These include efficient beamforming design [19, 20], resource allocation [21], optimized power beacon (PB) placement [22], and waveform design [23]. In addition, characteristics of the propagation environment is an important factor for wireless power transmission and the received power level depends on the range of frequencies used [24]. Accordingly, in the existing literature, depending on the nature of both the source that is used to harvest RF energy and the receiver architecture, three main approaches have been identified as (1) wireless energy harvesting, (2) wireless power transfer (WPT), and (3) simultaneous wireless information and power transfer (SWIPT).

- **Wireless energy harvesting:** This approach refers to harvesting energy from the ambient RF signals available in the environment. While solutions based on TV broadcasting, WiFi, and GSM signals have been developed, an issue with the approach is the variable nature of the ambient RF signal sources. Moreover, the approach is also sensitive to several factors such as path loss and shadowing effects as well as the choice of the rectifier since often a range of frequencies must be scanned in order to harvest sufficient amounts of energy.
- **Wireless power transfer:** WPT refers to harvesting energy using dedicated external sources such as a transmitter or a PB [18]. Available solutions to perform WPT can be divided into two categories: (1) near-field and (2) far-field. Popular methods of near-field WPT include inductive power transfer between nearby coils or magnetic resonance coupling. Although such methods exhibit high conversion efficiency, they are not suitable for mobile applications due to very short distances. On the other hand, far-field methods rely on the radiative nature of wave propagation. The history of far-field WPT can be traced back to Nicola Tesla's experiments in the last century. Although the experiments ended up in failure, they opened the way for more recent developments in microwave WPT [25].

The gains of WPT depend on several factors such as the placement of PBs and the ability of the antenna array to focus the radiated power in the desired user direction. Moreover, frequency of the signal used for WPT has an impact on the performance and the sharpness of the beam increases with the signal frequency. However, high frequency signals such as millimeter waves are subject to severe attenuation and blockage effects. Hence, an optimum frequency must be selected to achieve a high WPT efficiency.

- **Simultaneous wireless information and power transfer:** Varshney in [26] proposed a new form of WPT coined as SWIPT. In SWIPT, both information and RF energy are conveyed from the source to the destination and, therefore, SWIPT is suitable for low power operation. Also SWIPT saves spectrum by

simultaneously transmitting information and energy using the same waveform. Several researchers have looked into practical ways of implementing SWIPT receivers [19]. The two main architectures described in the literature include the time-switching (TS) receiver and power-splitting (PS) receiver. A TS receiver operates by allowing the terminal to adaptively switch between the information and energy receiver over orthogonal time periods. A PS receiver, on the other hand, splits the incoming RF signal into two streams with different power levels, one for information reception and one for energy harvesting. If multiple antennas are present, SWIPT architectures based on antenna switching can be implemented where antennas are divided into two disjoint sets, one for information reception and other for energy harvesting [27].

2.1.2 Full-Duplex Wireless-Powered Communications

FD and WPT can be combined to realize communications with improved performance. Several attractive features of FD wireless-powered communications include:

- In many cases of interest, FD wireless-powered systems exhibit higher throughput gains as compared to their HD counterparts.
- As shown in [28, 29], undesirable SI component can be converted into an extra source of energy harvesting in FD wireless-powered communications. Hence, FD radios that can recycle the energy of the transmitted signal can be designed. Also, it is beneficial to use multiple antennas to harvest practical amounts of energy [27]. This approach can be coupled with FD communications, since spatial-domain SI cancellation can be implemented for improved performance [7].
- A FD base station (BS) can receive information and transfer energy to a set of disjoint terminals at the same time. Such a possibility is helpful for rapidly responding to the energy demands of the terminals and efficiently managing the perpetual operation of the network [11, 30, 31].
- FD nodes capable of WPT are ideal for 5G small cell implementation. In general, FD radios are unable to transmit with very high power due to possible generation of SI, while path loss significantly limits the energy harvesting performance. Hence, FD and WPT when combined together will offer benefits in terms of the increased spectral and energy efficiency.

2.1.3 Recent Results

This subsection presents a comprehensive survey of the state-of-the-art techniques on FD wireless-powered communication systems. There are three main topologies investigated in the literature. The first topology refers to the case of FD bi-directional

communications where one or both nodes of the point-to-point system apply TS or PS architecture to perform energy harvesting and information decoding. In particular, so far FD WPT [32] and FD SWIPT [33–35] bi-directional systems have been studied. In [32], a multi-antenna bi-directional FD WPT system, in which a device powered by WPT from an energy transmitter communicates with an information receiver over the same frequency band, has been considered. Specifically, the achievable rate associated with the link from the device to the information receiver has been maximized by jointly optimizing the energy beamforming at the energy transmitter and information beamforming at the device subject to transmit power constraints. In [33], optimal transmit beamforming vector at a FD access point (AP), PS ratio at the FD mobile station (MS), and transmit power of the FD MS have been designed to minimize the system's weighted sum transmit power. However, authors in [33] have assumed perfect SI cancellation, and therefore, the effect of SI is not included in the results. In [34], an antenna pair selection scheme has been introduced to improve the performance of a FD wireless-powered bi-directional system. Optimum design of the PS ratio and transmit power for SWIPT, in a FD bi-directional communication system with dual-antenna nodes, was analyzed in [35]. The FD wireless-powered bi-directional system model has also been extended to include the cases of physical layer security in [36] and machine-to-machine communication for the internet-of-things (IoT) [37].

The second topology studied in the literature is the FD relay topology. To this end, [28, 38–43] have investigated the three-node FD relay channel and WPT. In [38], throughput of a single-antenna dual-hop FD relaying system, assuming a TS-based receiver, has been studied with the aim of characterizing the fundamental trade-off between the energy harvesting and communication periods. Note that most contemporary wireless standards promote the use of multiple antenna terminals, and hence there is a need to understand the performance under more general antenna setups [44]. The concept of “self-energy recycling” in the context of WPT has been proposed in [28, 29], where the FD node regains a portion of its own transmit energy via the SI channel. The integration of SI for WPT and optimal beamforming design at the relay have been studied in [39]. A FD multi-antenna relaying system with SWIPT has been considered in [40], where the source and relay transceiver have been designed based on the minimum mean-square-error criterion.

The incorporation of the harvest-use model and TS-based FD relaying have been considered in [41]. The results in [41] demonstrate that the FD mode can outperform the HD counterpart. PS-based FD relaying with the harvest-use and harvest-store-use models have been studied in [42], where the relay periodically switches between two rechargeable batteries for charging and discharging during two consecutive time slots of each block. The optimal PS ratio that maximizes the end-to-end signal-to-interference-plus-noise ratio (SINR) and the trade-off between the end-to-end SINR and recycled self-power have also been characterized. In [43], assuming a dual-hop FD relaying system, the PS parameter and energy consumption proportion in the case of single-antenna transceivers have been jointly optimized. As concluded in this study, self-energy recycling has a limited effect and relaying is useful only when the direct source-to-destination link is very weak.

The third topology presented in the literature is the FD hybrid AP topology where data from users in the uplink channel and energy to the users in the downlink channel are transmitted and received simultaneously [45–48]. The work in [45] considered a wireless-powered communication network, where a hybrid FD AP broadcasts energy to a set of users and receives information from another set of users via time-division multiple access at the same time. Under perfect and imperfect SI cancellation at the AP, the time allocation for the downlink energy transfer and the uplink information transfer and the transmit power allocation have been jointly optimized. The same system setup has been considered in [46], where a sum-throughput maximization problem and a total-time minimization problem have been studied. In [47], considering a multi-user scenario, the case of orthogonal frequency division multiplexing has been studied by jointly optimizing the subcarrier scheduling and power allocation. In [48], a resource allocation algorithm design for a SWIPT system consisting of a FD BS, multiple single-antenna HD users, and multiple energy harvesters equipped with multiple antennas has been presented. A FD multiuser multiple-input multiple-output (MIMO) system has been studied in [49], where uplink users first harvest energy via BS energy beamforming before transmitting their information to the BS, while at the same time the BS transmits information to the users in the downlink channel. The FD hybrid BS topology has also been extended to physical layer security in [50], where the transmitter covariance matrix and receive combining vector at the multi-antenna hybrid BS have been jointly optimized to maximize the weighted uplink and downlink secrecy sum rate. Hardware feasibility of FD and WPT has also been demonstrated in [51], where an AP and a sensor node transmit data to each other while the AP simultaneously delivers power to the sensor.

Table 2.1 shows the summary of recent results discussed above on FD wireless-powered communication systems.

2.1.4 Chapter Organization

The aim of this chapter is to analyze and optimize the performance of FD wireless-powered communications. The presented analysis considers general multiple antenna setups, while the effect of residual SI is modeled specifically to show the corresponding performance insights of practical significance. In particular, we consider bi-directional, relay, and hybrid AP enabled FD wireless-powered communications with precoder design and parameter optimization in Sects. 2.2–2.4, respectively. In Sect. 2.5 we discuss future research challenges related to FD wireless-powered communications and conclusions are drawn in Sect. 2.6.

Notation: We use bold upper case letters to denote matrices, bold lower case letters to denote vectors. $\|\cdot\|$, $(\cdot)^\dagger$, $(\cdot)^{-1}$, and $\text{tr}(\cdot)$ to denote the Euclidean norm, conjugate transpose operator, matrix inverse, and the trace of a matrix, respectively;

Table 2.1 Summary of recent results on FD wireless-powered communication systems

Literature	Topology	Wireless energy transfer receiver technique	Architecture	Design objective
[32]	Bi-directional	WPT	TS	Maximizing the achievable rate
[33]	Bi-directional	SWIPT	PS	Minimizing the sum transmit power
[34]	Bi-directional	SWIPT	–	Antenna pair selection
[35]	Bi-directional	SWIPT	PS	Maximizing the sum rate
[36]	Bi-directional	SWIPT	TS	Improving the physical layer security
[28]	Relay (AF)	SWIPT	TS	Maximizing the throughput. Self-energy recycling is assumed
[38]	Relay (AF/DF)	SWIPT	TS	Optimizing the TS parameter
[39, 40]	Relay (AF)	SWIPT	TS-PS	Beamforming optimization
[41]	Relay (AF/DF)	SWIPT	TS	Maximizing the channel capacity
[42]	Relay (DF)	SWIPT	PS	Maximizing the e2e SINR
[43, 44]	Relay (DF)	SWIPT	PS-TS	Maximizing the information rate
[45–47]	AP	WPT	–	Maximizing the sum-throughput of uplink transmissions
[48]	AP	WPT	–	Minimizing the uplink/downlink transmit power
[49]	AP	WPT	TS	Maximizing the sum rate
[50]	AP	WPT	–	Maximizing the weighted sum secrecy rate

$\Pr(\cdot)$ denotes the probability; $f_X(\cdot)$ and $F_X(\cdot)$ denote the probability density function (pdf) and cumulative distribution function (cdf) of the random variable (RV) X , respectively; $\mathcal{CN}(\mu, \sigma^2)$ denotes a circularly symmetric complex Gaussian RV x with mean μ and variance σ^2 ; $W(x)$ is the Lambert W -function, defined as the solution for W in $W \exp(W) = x$ [52]; $\Gamma(a)$ is the Gamma function; $\Gamma(a, x)$ is upper incomplete Gamma function [53, Eq. (8.350)]; $K_\nu(\cdot)$ is the ν th order modified Bessel function of the second kind [53, Eq. (8.432)]; $\psi(x)$ is the psi (digamma) function [53, Eq. (8.360.1)]; $E_n(x)$ is the E_n -function [53], and $G_{pq}^{mn} \left(z \mid \begin{smallmatrix} a_1 \cdots a_p \\ b_1 \cdots b_q \end{smallmatrix} \right)$ denotes the Meijer G-function [53, Eq. (9.301)].

2.2 Full-Duplex Wireless-Powered Bi-directional Communications

In this section, we propose optimum and suboptimum schemes to enlarge the boundary of the BS-MS rate region for a FD wireless-powered bi-directional communication system.

2.2.1 System Model

As shown in Fig. 2.1, we consider FD bi-directional communications between an N -antenna BS and a MS with two antennas [54]. Specifically, the BS has M_T transmit antennas and $(N - M_T)$ receive antennas. At the MS side, one antenna is used for transmission and the other for reception. Since the MS is usually power limited and the uplink rate is the bottleneck, we consider a case where the BS first transmits energy to the MS, which will be used by the MS for the subsequent uplink transmission.

The communication takes place in two phases with duration α and $(1-\alpha)$, respectively. In phase I, the BS transmits energy to the MS. Suppose the transmit power of BS in this phase is P_{BS} , then the received energy is $E = \alpha P_{BS} \lambda(\mathbf{H}_{BM} \mathbf{H}_{BM}^\dagger)$, where the channel between the BS and the MS is denoted as \mathbf{H}_{BM} and $\lambda(\cdot)$ returns the maximum eigenvalue of a matrix. In phase II, the BS and the MS communicate to each other using FD operation. The MS's transmit power can be written as $p_m = \kappa P_{BS} \lambda(\mathbf{H}_{BM} \mathbf{H}_{BM}^\dagger)$ with $\kappa \triangleq \frac{\alpha \eta}{1-\alpha}$ where η is RF-to-DC energy conversion efficiency coefficient. The conversion efficiency, and thus the coefficient value depends on several factors, such as the efficiency of the rectenna and power efficiency of the hardware circuit that converts the received RF signals to DC voltage [15]. The

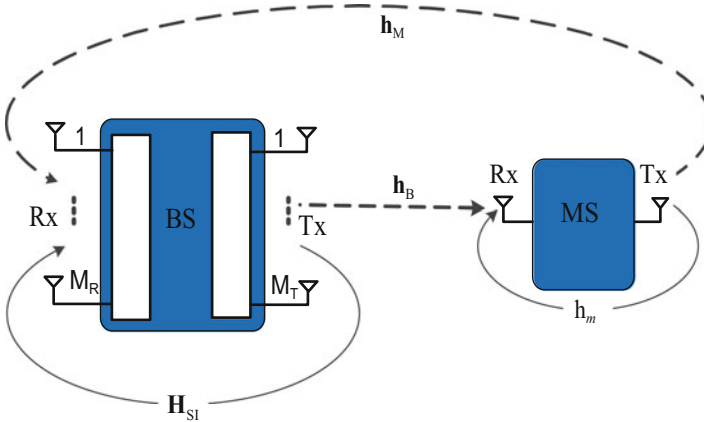


Fig. 2.1 FD wireless-powered bi-directional communication system

channels from the BS to MS and from the MS to BS are denoted by $\mathbf{h}_B^\dagger \in \mathbb{C}^{1 \times M_T}$ and $\mathbf{h}_M \in \mathbb{C}^{(N-M_T) \times 1}$, respectively. FD operation causes SI at the BS and MS receive antennas. The SI channels are $\mathbf{H}_{\text{SI}} \in \mathbb{C}^{(N-M_T) \times M_T}$ and h_M at the BS and MS, respectively. The transmit beamformer at the BS is \mathbf{w}_t and the noise power at the BS and MS is denoted by σ_b^2 and σ_m^2 , respectively.

By using the minimum mean-square-error receiver at the BS, the BS and MS achievable rates are, respectively, calculated as [54]

$$r_B = (1 - \alpha) \log_2 \left(1 + \frac{p_m}{\sigma_b^2} \left(\|\mathbf{h}_M\|^2 - \frac{|\mathbf{h}_M^\dagger \mathbf{H}_{\text{SI}} \mathbf{w}_t|^2}{\sigma_b^2 + \|\mathbf{H}_{\text{SI}} \mathbf{w}_t\|^2} \right) \right), \quad (2.1)$$

$$r_M = (1 - \alpha) \log_2 \left(1 + \frac{|\mathbf{h}_B^\dagger \mathbf{w}_t|^2}{\sigma_m^2 + p_m |h_m|^2} \right). \quad (2.2)$$

The maximum achievable rate at the BS has been derived in [54] as

$$R_B^{\max} = (1 - \alpha^*) \log_2 \left(1 + \frac{\alpha^*}{1 - \alpha^*} \frac{b \|\mathbf{h}_M\|^2}{\sigma_b^2} \right), \quad (2.3)$$

where $\alpha^* = \left(\exp \left(W \left(\frac{\tilde{b}-1}{e} \right) + 1 \right) - 1 \right) / \left(\tilde{b} + \exp \left(W \left(\frac{\tilde{b}-1}{e} \right) + 1 \right) - 1 \right)$ and $\tilde{b} = b \frac{\|\mathbf{h}_M\|^2}{\sigma_b^2}$ with $b = \eta P_{\text{BS}} \lambda \left(\mathbf{H}_{\text{BM}} \mathbf{H}_{\text{BM}}^\dagger \right)$. The MS-BS rate region can be obtained by maximizing the MS rate while confirming that the BS-rate is equal to a certain value R_B . By solving this optimization problem for all R_B , where $R_B \in [0, R_B^{\max}]$ and R_B^{\max} is the maximum value of BS rate, we obtain the MS-BS rate region. As such, the optimization problem for a given R_B is expressed as

$$\begin{aligned} & \max_{\|\mathbf{w}_t\|^2 \leq P_{\text{BS}}, 0 \leq \alpha \leq 1, p_m} (1 - \alpha) \log_2 \left(1 + \frac{|\mathbf{h}_B^\dagger \mathbf{w}_t|^2}{\sigma_m^2 + p_m |h_m|^2} \right) \\ & \text{s.t.} \quad (1 - \alpha) \log_2 \left(1 + \frac{p_m}{\sigma_b^2} \left(\|\mathbf{h}_M\|^2 - \frac{|\mathbf{h}_M^\dagger \mathbf{H}_{\text{SI}} \mathbf{w}_t|^2}{\sigma_b^2 + \|\mathbf{H}_{\text{SI}} \mathbf{w}_t\|^2} \right) \right) = R_B, \\ & \quad p_m = \frac{\alpha \eta P_{\text{BS}} \lambda \left(\mathbf{H}_{\text{BM}} \mathbf{H}_{\text{BM}}^\dagger \right)}{(1 - \alpha)}. \end{aligned} \quad (2.4)$$

The optimization problem (2.4) is a complicated non-convex optimization with respect to (w.r.t.) \mathbf{w}_t and α . However, (2.4) can be solved efficiently by finding optimum \mathbf{w}_t for a given α and vice-versa. Since α is scalar valued, the optimum solution can be ascertained by using one-dimensional search w.r.t. α .

2.2.2 Joint Optimization of Beamformer and Time-Splitting Parameter

In this subsection, optimum and suboptimum schemes for solving the joint optimization of the beamformer, \mathbf{w}_t , and TS parameter, α , are presented.

2.2.2.1 Optimum Scheme

The optimum scheme corresponds to finding \mathbf{w}_t that maximizes the end to end SINR for a given α . Since α is scalar valued, the jointly optimal solution of \mathbf{w}_t and α can be obtained by using one-dimensional search w.r.t. α . The computational complexity of line search is minimized by exploiting the nature of the optimization problem (2.4).

1. *Optimization of \mathbf{w}_t* : First consider the problem of optimizing \mathbf{w}_t for a given α . In this case, the optimization problem (2.4) is expressed as

$$\begin{aligned} \max_{\|\mathbf{w}_t\|^2 \leq P_{BS}} \quad & (1 - \alpha) \log \left(1 + \frac{|\mathbf{h}_B^\dagger \mathbf{w}_t|^2}{\sigma_m^2 + p_m |h_m|^2} \right) \\ \text{s.t.} \quad & (1 - \alpha) \log_2 \left(1 + \frac{p_m}{\sigma_b^2} \left(\|\mathbf{h}_M\|^2 - \frac{|\mathbf{h}_M^\dagger \mathbf{H}_{SI} \mathbf{w}_t|^2}{\sigma_b^2 + \|\mathbf{H}_{SI} \mathbf{w}_t\|^2} \right) \right) = R_B. \end{aligned} \quad (2.5)$$

Since $\log(1 + x)$ is a monotonically increasing function of $x \triangleq \frac{|\mathbf{h}_B^\dagger \mathbf{w}_t|^2}{\sigma_m^2 + p_m |h_m|^2}$ and the denominator, $\sigma_m^2 + p_m |h_m|^2$, of x is independent of \mathbf{w}_t , (2.5) can be solved from

$$\max_{\|\mathbf{w}_t\|^2 \leq P_{BS}} |\mathbf{h}_B^\dagger \mathbf{w}_t|^2 \quad \text{s.t.} \quad \frac{|\mathbf{h}_M^\dagger \mathbf{H}_{SI} \mathbf{w}_t|^2}{\sigma_b^2 + \|\mathbf{H}_{SI} \mathbf{w}_t\|^2} = \Gamma_B, \quad (2.6)$$

where $\Gamma_B \triangleq \|\mathbf{h}_M\|^2 - \frac{\sigma_b^2}{p_m} \left[2^{\frac{R_B}{1-\alpha}} - 1 \right]$. It is clear that the objective function in (2.6) is maximized with $\|\mathbf{w}_t\|^2 = P_{BS}$. This optimization problem is non-convex due to the fact that it is the maximization of a quadratic function with a quadratic equality constraint. Moreover, (2.6) does not admit a closed-form solution. However, it can be efficiently and optimally solved using semi-definite programming. For this purpose, define $\mathbf{V}_B \triangleq \mathbf{w}_t \mathbf{w}_t^\dagger$ and relax the rank-one constraint, $\text{rank}(\mathbf{V}_B) = 1$. The relaxed optimization is

$$\begin{aligned} \max_{\mathbf{V}_B} \quad & f(\alpha, p_m) = \text{tr}(\mathbf{V}_B \mathbf{h}_B \mathbf{h}_B^\dagger) \\ \text{s.t.} \quad & \text{tr}(\mathbf{V}_B \mathbf{H}_{SI}^\dagger \mathbf{h}_M \mathbf{h}_M^\dagger \mathbf{H}_{SI}) = \Gamma_B \left(\sigma_b^2 + \text{tr}(\mathbf{V}_B \mathbf{H}_{SI}^\dagger \mathbf{H}_{SI}) \right), \end{aligned}$$

$$\text{tr}(\mathbf{V}_B) = P_{BS}, \mathbf{V}_B \succeq 0. \quad (2.7)$$

The optimization problem (2.7) is a standard semi-definite relaxation (SDR) problem with only two equality constraints. Therefore, according to Shapiro–Barvinok–Pataki (SBP) rank reduction theorem [55], there exists a rank-one optimum solution of \mathbf{V}_B . Let \mathbf{V}_B^* be the optimum solution of (2.7). Since \mathbf{V}_B^* is rank-one matrix, the optimum solution \mathbf{w}_t^* is obtained $\mathbf{w}_t^* = \sqrt{P_{BS}} \tilde{\mathbf{u}} \tilde{\mathbf{u}}^\dagger$, where $\tilde{\mathbf{u}}$ is the eigenvector corresponding to a non-zero eigenvalue of \mathbf{V}_B^* .

2. *Optimization of \mathbf{w}_t and α :* In order to jointly optimize \mathbf{w}_t and α , the SDR problem (2.7) can be solved using an one-dimensional (or line search) search over α where $0 \leq \alpha \leq 1$. However, this line search can be limited to a small segment, and therefore the number of required SDR optimizations can be significantly minimized. To illustrate this, let the objective function in (2.5), for a given \mathbf{w}_t^* , be defined as

$$f(\alpha) = (1 - \alpha) \log_2 \left(1 + \frac{\mu}{c + \frac{\alpha b}{1 - \alpha}} \right), \quad (2.8)$$

where $\mu = \frac{|\mathbf{h}_B^\dagger \mathbf{w}_t^*|^2}{|\mathbf{h}_m|^2}$ and $c = \frac{\sigma_m^2}{|\mathbf{h}_m|^2}$. The derivative of $f(\alpha)$ can be written as

$$\frac{df(\alpha)}{d\alpha} = -\log_2(g(\alpha)) - \frac{b\mu g(\alpha)^{-1}}{(1 - \alpha) \log(2)} \left(c + \frac{\alpha b}{1 - \alpha} \right)^{-2}, \quad (2.9)$$

where $g(\alpha) = 1 + \frac{\mu}{c + \frac{\alpha b}{1 - \alpha}} \geq 0, \forall \alpha \in [0, 1]$. It is clear from (2.9) that $\frac{df(\alpha)}{d\alpha} < 0$ for all α , i.e., $f(\alpha)$ is a monotonically decreasing function of α . This means that the maximum value of the objective function is achieved when α is minimum, provided that the equality constraint is fulfilled. However, as $\alpha \rightarrow 0$, $\Gamma_B \rightarrow \infty$, i.e., the infeasibility of the SDR optimization problem (2.7) increases. Consequently, the optimum α is the minimum α for which (2.7) is feasible. The output \mathbf{V}_B of such feasible SDR provides the optimum \mathbf{w}_B . In a nutshell, the proposed optimum solution can be summarized as follows:

1. Define a fine grid of α in steps of $\partial\alpha$. Start with $\alpha = 0$.
2. Solve (2.7) with the increment of $\partial\alpha$.
3. If feasible, stop and output α and \mathbf{V}_B .
4. If not, go to step (2).

2.2.2.2 Suboptimal Scheme

The scheme presented in Sect. 2.2.2.1 requires an extensive optimization. Hence, in order to find a low-complexity closed-form solution, we can enforce a ZF constraint so that the designed transmit beamformer \mathbf{w}_t ensures no SI for the FD operation at the BS. To realize this, it is easy to check from (2.4) that the following condition is sufficient,

$$\mathbf{w}_t^\dagger \mathbf{H}_{\text{SI}}^\dagger \mathbf{h}_M = 0. \quad (2.10)$$

1. *Optimization of \mathbf{w}_t* : Substituting (2.10) into (2.4), the resulting optimization problem for a given α can be re-expressed as [54]

$$\begin{aligned} \max_{\mathbf{w}_t} \quad & |\mathbf{h}_B^\dagger \mathbf{w}_t|^2 \\ \text{s.t.} \quad & \|\mathbf{w}_t\|^2 \leq P_{\text{BS}} \\ & \mathbf{w}_t^\dagger \mathbf{H}_{\text{SI}}^\dagger \mathbf{h}_M = 0. \end{aligned} \quad (2.11)$$

Using a standard Lagrangian multiplier method and skipping the corresponding details, the closed-form solution of \mathbf{w}_t is expressed as $\mathbf{w}_t^* = \sqrt{P_{\text{BS}}} \frac{\mathbf{B} \mathbf{h}_B}{\|\mathbf{B} \mathbf{h}_B\|}$ where

$$\mathbf{B} = \mathbf{I} - \frac{\mathbf{H}_{\text{SI}}^\dagger \mathbf{h}_M \mathbf{h}_M^\dagger \mathbf{H}_{\text{SI}}}{\|\mathbf{H}_{\text{SI}}^\dagger \mathbf{h}_M\|^2}.$$

Accordingly, the corresponding objective function becomes $|\mathbf{h}_B^\dagger \mathbf{w}_t|^2 = P_{\text{BS}} \|\mathbf{B} \mathbf{h}_B\|^2$.

2. *Optimization of α* : Obviously, the transmit beamformer \mathbf{w}_t^* is independent of α . Therefore, the optimization problem (2.4) w.r.t. α is equivalent to

$$\begin{aligned} \max_{0 \leq \alpha \leq 1} \quad & f(\alpha) \triangleq (1 - \alpha) \log_2 \left(1 + \frac{\mu}{c + \frac{\alpha b}{1 - \alpha}} \right) \\ \text{s.t.} \quad & (1 - \alpha) \log_2 \left(1 + \frac{\alpha}{1 - \alpha} \tilde{b} \right) = R_B. \end{aligned} \quad (2.12)$$

The optimum α would be zero if there were no equality constraint (or the constraint with $R_B = 0$). In the presence of equality constraint with $R_B > 0$, it is clear that the optimum α is the smallest α that satisfies the equality constraint. The following proposition presents α .

Proposition 1. *When equality constraint is feasible (i.e., $R_B \leq R_B^{\max}$), the optimum α is given by*

$$\alpha^{\text{opt}} = \frac{-\frac{1}{R_B \log(2)} W \left(-\frac{R_B \log(2)}{b\gamma} e^{R_B \log(2) \left(1 - \frac{1}{b}\right)} \right) - \frac{1}{b}}{1 - \frac{1}{R_B \log(2)} W \left(-\frac{R_B \log(2)}{\tilde{b}} e^{R_B \log(2) \left(1 - \frac{1}{b}\right)} \right) - \frac{1}{\tilde{b}}}. \quad (2.13)$$

Proof. The equality constraint for the BS rate is expressed as

$$\log \left(1 + \frac{\alpha}{1 - \alpha} \tilde{b} \right) = R_B \log(2) \left(\frac{\alpha}{1 - \alpha} + 1 \right). \quad (2.14)$$

Define $y \triangleq 1 + \frac{\alpha}{1-\alpha}b$. Then, after simple manipulations, (2.14) can be expressed as

$$\left(-\frac{R_B \log(2)}{\tilde{b}}y\right) e^{-\frac{R_B \log(2)}{\tilde{b}}y} = \left(-\frac{R_B \log(2)}{\tilde{b}}\right) e^{R_B \log(2)\left(1-\frac{1}{\tilde{b}}\right)}. \quad (2.15)$$

Using the Lambert-W function, y in (2.15) is expressed as

$$y = \frac{-\tilde{b}}{R_B \log(2)} W\left(-\frac{R_B \log(2)}{\tilde{b}} e^{R_B \log(2)\left(1-\frac{1}{\tilde{b}}\right)}\right). \quad (2.16)$$

Note that $\frac{R_B \log(2)}{\tilde{b}} e^{R_B \log(2)\left(1-\frac{1}{\tilde{b}}\right)} \leq \frac{1}{e}$ is required to have a real value of y . If not, the equality constraint is not feasible for given \tilde{b} and R_B where $R_B \leq R_B^{\max}$. Substituting y in (2.16), we obtain

$$\frac{\alpha}{1-\alpha} = \frac{-1}{R_B \log(2)} W\left(-\frac{R_B \log(2)}{\tilde{b}} e^{R_B \log(2)\left(1-\frac{1}{\tilde{b}}\right)}\right) - \frac{1}{\tilde{b}}$$

which yields the optimum α^{Opt} given in (2.13).

We now corroborate our analysis with the numerical examples to reveal the behavior of the MS-BS rate region. The distance between the BS and MS is set to 10 meters, whereas the path loss exponent is taken as 3. The noise powers, σ_b^2 and σ_m^2 , are fixed to -70 dBm. Figure 2.2 shows the rate regions obtained with the optimum and suboptimum methods for $M_T = 2$ and 3, when $N = 5$, $P_{\text{BS}} = 30$ dBm, whereas the corresponding regions for $P_{\text{BS}} = 0$ dBm are shown in Fig. 2.3. The channel coefficients (excluding the path attenuation) for all channels are taken as independent and identically distributed (i.i.d.) $\mathcal{CN}(0, 1)$ RVs. All results correspond to averaging of 100 independent channel realizations. The BS rate is varied from 0 to R_B^{\max} . The achieved BS-MS rate regions are also shown for the HD mode. Note that, in the HD mode, the information transmission period of $(1-\alpha)$ is equally divided for the BS to MS and then the MS to BS communications. Due to the HD protocol, the BS and MS can utilize all of their antennas for transmit and receive beamforming as in standard MIMO communications. Thus, the BS and MS information rates are, respectively, given by

$$\begin{aligned} r_{B,H} &= \frac{1-\alpha}{2} \log_2 \left(1 + \frac{\alpha}{1-\alpha} \frac{\eta P_{\text{BS}} \lambda^2 (\mathbf{H}_{\text{BM}} \mathbf{H}_{\text{BM}}^\dagger)}{\sigma_b^2} \right), \\ r_{M,H} &= \frac{1-\alpha}{2} \log_2 \left(1 + \frac{P_{\text{BS}} \lambda (\mathbf{H}_{\text{BM}} \mathbf{H}_{\text{BM}}^\dagger)}{\sigma_m^2} \right). \end{aligned} \quad (2.17)$$

It can be observed from Figs. 2.2 and 2.3 that the maximum value of the MS rate is obtained when R_B is minimum, whereas the minimum value is obtained when R_B takes maximum value. Moreover, the BS-rate is much smaller than the MS-

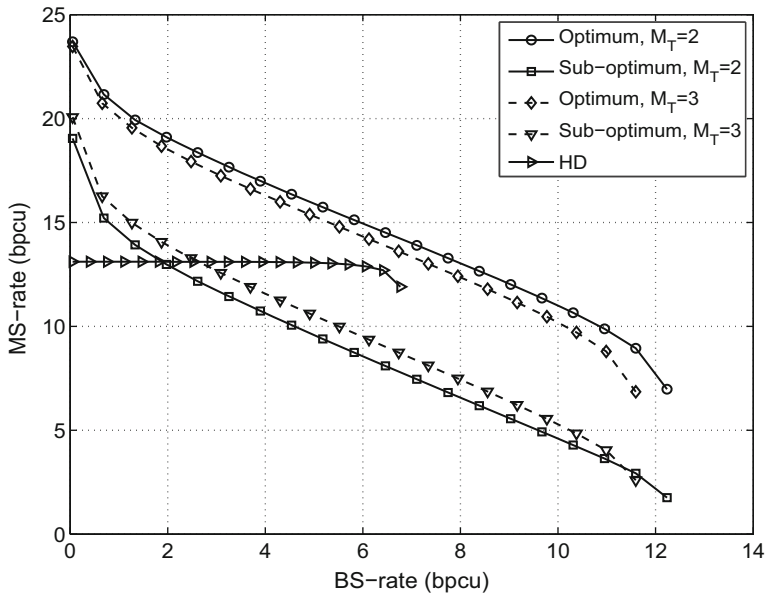


Fig. 2.2 MS-BS rate region with $P_{BS} = 30$ dBm, and $M_T = 2, 3$

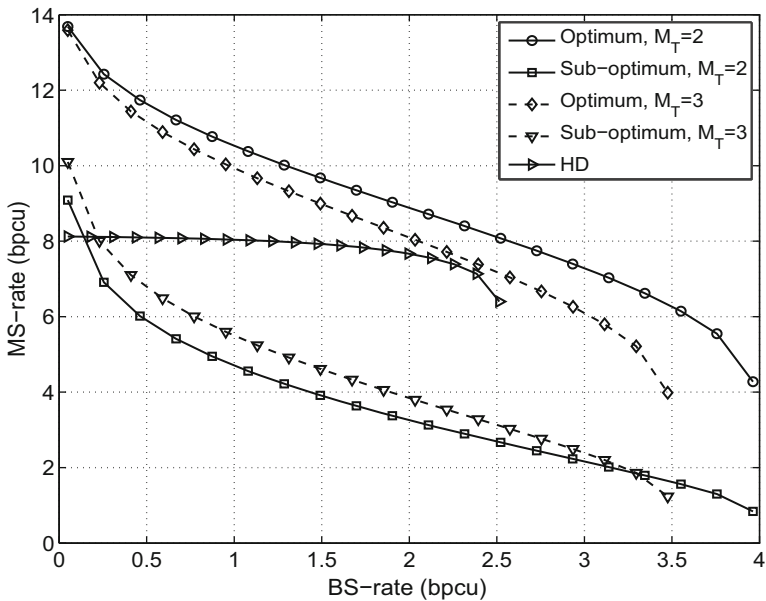


Fig. 2.3 MS-BS rate region with $P_{BS} = 0$ dBm, $M_T = 2, 3$, and $N = 5$

rate. This is due to the fact that the former is limited by the transmit power of the MS which depends on the harvested power. Both figures show that the optimum method performs much better than the suboptimum approach. Moreover, when M_T increases, the obtained maximum BS rate decreases, whereas the maximum MS rate remains almost unchanged in the optimum method and increases in the suboptimum method. Figure 2.2 shows that the maximum BS and MS rates obtained with the optimum method are almost double of the corresponding rates of the HD mode. However, when the BS rate increases, the MS rate decreases rapidly in the FD mode, whereas it only decreases gradually in the HD mode. The advantage of the FD mode over the HD mode diminishes as P_{BS} decreases, as seen from Fig. 2.3. As a final observation, the advantage of the optimum method is more pronounced for smaller values of M_T .

2.3 Full-Duplex Wireless-Powered Relay Communications

The source-relay-destination topology is another widely considered system model in the current FD literature [1]. When FD relays are employed, information from the source can be transferred to the destination in one time slot, and thus the spectral efficiency bottleneck of using HD relays can be resolved. FD operation of the relays offers clear benefits for use in modern wireless networks [56]. As an example, the self-backhauling capability of FD relays has been identified as a useful feature for their use in dense 5G indoor networks [57]. Furthermore, FD relays with limited transmit power can be carefully placed in order to cover coverage gaps, although several relays would be required. While important results on FD relays with fixed and reliable power supplies have been reported in the literature, as outlined in Sect. 2.1.3, FD wireless-powered relay communications is still in infancy and deserves more investigation.

Consider a two-hop FD decode-and-forward relay system where the relay is powered using WPT from the source signals. Specifically, below we design optimum and suboptimum receive and transmit beamformers at the multiple antenna relay and optimize the TS parameter to characterize the instantaneous throughput and delay-constrained throughput.

2.3.1 System Model

Figure 2.4 shows a FD decode-and-forward relay system consisting of one source S , one relay R , and one destination, D [44]. Both S and D are equipped with a single antenna, while R is equipped with two sets of antennas, i.e., M_R receiving antennas and M_T transmitting antennas. The relay has no external power supply and employs the TS protocol to receive energy from S . Hence, the entire communication process is divided into two phases, i.e., for a transmission block time T , α fraction

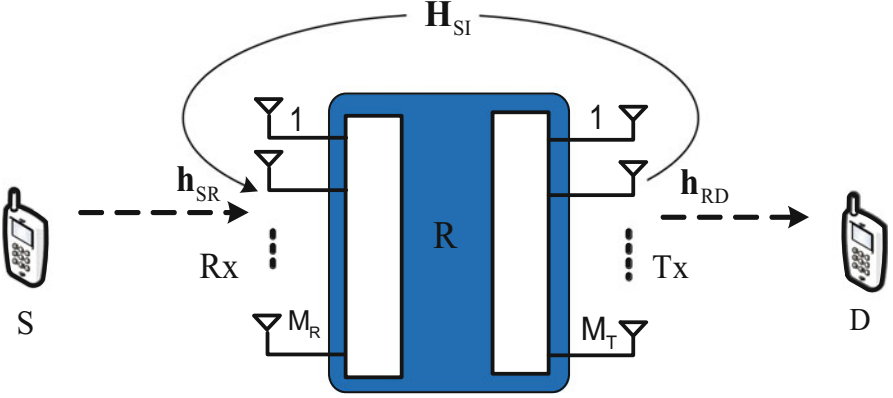


Fig. 2.4 FD wireless-powered relay system model

of the block time is devoted for energy harvesting and the remaining time, $(1 - \alpha)T$, is used for information transmission. We assume that the channels in the two-hop system remain constant over the block time T and vary independently from one block to the other. Such a fading process is known as block fading in the literature. We denote the channel coefficient from S to R and from R to D by $\mathbf{h}_{SR} \in \mathbb{C}^{M_R \times 1}$ and $\mathbf{h}_{RD} \in \mathbb{C}^{1 \times M_T}$, respectively.

The relay uses the harvested energy during αT period for subsequent transmission to D . Therefore, the transmit power of R is given by

$$P_r = \kappa P_S \beta_1 \|\mathbf{h}_{SR}\|^2, \quad (2.18)$$

where P_S is the source transmit power and β_1 models the path loss effect in S - R channel.

At the information transmission phase, upon receiving source signal, R applies a linear combining vector \mathbf{w}_r , then forwards the estimated signal to D using the transmit beamforming vector \mathbf{w}_t . Hence, end to end SINR at D can be expressed as [44]

$$\gamma_{FD} = \min \left(\frac{\bar{\gamma}_1 \beta_1 |\mathbf{w}_r^\dagger \mathbf{h}_{SR}|^2}{\kappa \bar{\gamma}_1 \beta_1 \|\mathbf{h}_{SR}\|^2 |\mathbf{w}_r^\dagger \mathbf{H}_{SI} \mathbf{w}_t|^2 + 1}, \kappa \bar{\gamma}_2 \beta_2 \|\mathbf{h}_{SR}\|^2 |\mathbf{h}_{RD} \mathbf{w}_t|^2 \right), \quad (2.19)$$

with $\bar{\gamma}_1 = \frac{P_S}{\sigma_R^2}$ and $\bar{\gamma}_2 = \frac{P_S}{\sigma_D^2}$ where σ_R^2 and σ_D^2 are the noise power at R and D , respectively, β_2 models the path loss effect for the R - D link, and $\mathbf{H}_{SI} \in \mathbb{C}^{M_R \times M_T}$ represents the residual SI channel whose elements are modeled as circularly symmetric complex Gaussian $\mathcal{CN}(0, \sigma_{SI}^2)$ RVs in line with the literature [3, 6]. Note that the SINR in (2.19) has a much more complicated form than the corresponding SINR in conventional relay networks having nodes with fixed power supplies, since

the signal received is subject to “double fading” due to channel fading during the energy harvesting and information transmission phases.

We now present the following optimization problem to maximize the instantaneous rate w.r.t. α , \mathbf{w}_t , and \mathbf{w}_r :

$$\max_{\|\mathbf{w}_r\|=\|\mathbf{w}_t\|=1, \alpha \in [0,1]} R(\alpha, \mathbf{w}_t, \mathbf{w}_r) = (1 - \alpha) \log_2 (1 + \gamma_{FD}). \quad (2.20)$$

2.3.2 Relay Beamforming Designs

The optimization problem (2.20) is non-convex and challenging to solve. To this end, we consider the beamforming design problem for a given α . In this case, (2.20) turns to a problem of maximizing the minimum of the first hop SINR and second-hop signal-to-noise ratio (SNR), which is expressed as

$$\max_{\|\mathbf{w}_r\|=\|\mathbf{w}_t\|=1} \min \left(\frac{\bar{\gamma}_1 \beta_1 |\mathbf{w}_r^\dagger \mathbf{h}_{SR}|^2}{\kappa \bar{\gamma}_1 \beta_1 \|\mathbf{h}_{SR}\|^2 |\mathbf{w}_r^\dagger \mathbf{H}_{S1} \mathbf{w}_t|^2 + 1}, \kappa \bar{\gamma}_2 \beta_1 \beta_2 \|\mathbf{h}_{SR}\|^2 |\mathbf{h}_{RD} \mathbf{w}_t|^2 \right). \quad (2.21)$$

In the following subsections, we provide optimum as well as suboptimum schemes for solving (2.21). In the optimum approach, the problem of joint transmit and receive beamforming design is considered, whereas in the suboptimum schemes, different linear receiver/transmitter techniques are employed at R .

2.3.2.1 Optimum Scheme

The optimum scheme corresponds to finding \mathbf{w}_r and \mathbf{w}_t such that the end to end SINR is maximized. Since the second-hop SNR does not depend on \mathbf{w}_r , the first-hop SINR can be maximized w.r.t \mathbf{w}_r by fixing \mathbf{w}_t . This optimization problem is a generalized Rayleigh ratio problem which is globally maximized when $\mathbf{w}_r = \frac{\mathbf{A}^{-1} \mathbf{h}_{SR}}{\|\mathbf{A}^{-1} \mathbf{h}_{SR}\|}$ where $\mathbf{A} = (\kappa \bar{\gamma}_1 \beta_1 \|\mathbf{h}_{SR}\|^2 \mathbf{H}_{S1} \mathbf{w}_t \mathbf{w}_t^\dagger \mathbf{H}_{S1}^\dagger + \mathbf{I})$. Accordingly, by substituting \mathbf{w}_r into (2.21), the corresponding problem can be solved and the $\mathbf{w}_t^{\text{OPT}}$ is given in [44, Proposition 1].

2.3.2.2 TZF Scheme

We now present some suboptimum beamforming solutions. One such scheme takes the advantage of the multiple transmit antennas to completely cancel the SI [58]. To ensure this is feasible, the number of the transmit antennas at relay should be greater than one, i.e., $M_T > 1$. In addition, maximal ratio combining (MRC) is

applied at the relay input, i.e., $\mathbf{w}_r^{\text{MRC}} = \frac{\mathbf{h}_{SR}}{\|\mathbf{h}_{SR}\|}$. This solution is named as the transmit zero-forcing (TZF) scheme in [44]. After substituting $\mathbf{w}_r^{\text{MRC}}$ into (2.21), the optimal transmit beamforming vector \mathbf{w}_t is obtained by solving the following problem:

$$\max_{\|\mathbf{w}_t\|=1} |\mathbf{h}_{RD}\mathbf{w}_t|^2, \quad \text{s.t.} \quad \mathbf{h}_{SR}^\dagger \mathbf{H}_{SI} \mathbf{w}_t = 0. \quad (2.22)$$

From the ZF constraint in (2.22), we know that \mathbf{w}_t lies in the null space of $\mathbf{h}_{SR}^\dagger \mathbf{H}_{SI}$. Denoting $\mathbf{B} \triangleq \mathbf{I} - \frac{\mathbf{H}_{SI}^\dagger \mathbf{h}_{SR} \mathbf{h}_{SR}^\dagger \mathbf{H}_{SI}}{\|\mathbf{h}_{SR}^\dagger \mathbf{H}_{SI}\|^2}$, we have $\mathbf{w}_t^{\text{ZF}} = \frac{\mathbf{B} \mathbf{h}_{RD}}{\|\mathbf{B} \mathbf{h}_{RD}\|}$. Now, substituting the \mathbf{w}_t^{ZF} and $\mathbf{w}_r^{\text{MRC}}$ into (2.19), the end-to-end SNR can be expressed as [44]

$$\gamma_{\text{TZF}} = \frac{\bar{\gamma}_1 \beta_1 \|\mathbf{h}_{SR}\|^2}{(1 - \alpha)} \min \left(1 - \alpha, \frac{\bar{\gamma}_2}{\bar{\gamma}_1} \eta \alpha \beta_2 \|\tilde{\mathbf{h}}_{RD}\|^2 \right), \quad (2.23)$$

where $\tilde{\mathbf{h}}_{RD}$ is an $(M_T - 1) \times 1$ vector and follows the chi-square distribution with $2(M_T - 1)$ degrees-of-freedom.

2.3.2.3 RZF Scheme

As an alternative solution, the transmit beamforming vector can be set using the maximal ratio transmit (MRT) principle, i.e., $\mathbf{w}_t^{\text{MRT}} = \frac{\mathbf{h}_{RD}}{\|\mathbf{h}_{RD}\|}$, and \mathbf{w}_r can be designed with the ZF criterion $\mathbf{w}_r^\dagger \mathbf{H}_{SI} \mathbf{w}_t = 0$. This solution is named as the receive ZF (RZF) scheme in [44]. To ensure feasibility of RZF, R should be equipped with $M_R > 1$ receive antennas. Substituting the MRT solution for \mathbf{w}_t into (2.21), the optimal receive beamforming vector \mathbf{w}_r is the solution to the following problem:

$$\max_{\|\mathbf{w}_r\|=1} |\mathbf{w}_r^\dagger \mathbf{h}_{SR}|^2 \quad \text{s.t.} \quad \mathbf{w}_r^\dagger \mathbf{H}_{SI} \mathbf{h}_{RD}^\dagger = 0. \quad (2.24)$$

Using similar steps as in the TZF scheme, the vector \mathbf{w}_r can be obtained as $\mathbf{w}_r^{\text{ZF}} = \frac{\mathbf{D} \mathbf{h}_{SR}}{\|\mathbf{D} \mathbf{h}_{SR}\|}$, where $\mathbf{D} \triangleq \mathbf{I} - \frac{\mathbf{H}_{SI} \mathbf{h}_{RD}^\dagger \mathbf{h}_{RD} \mathbf{H}_{SI}^\dagger}{\|\mathbf{H}_{SI} \mathbf{h}_{RD}\|^2}$ is the projection idempotent matrix with rank $(M_T - 1)$. Invoking (2.19), and using \mathbf{w}_r^{ZF} and $\mathbf{w}_t^{\text{MRT}}$, the end-to-end SNR can be expressed as [44]

$$\gamma_{\text{RZF}} = \min \left(\bar{\gamma}_1 \beta_1 \|\tilde{\mathbf{h}}_{SR}\|^2, \kappa \bar{\gamma}_2 \beta_1 \beta_2 \|\mathbf{h}_{SR}\|^2 \|\mathbf{h}_{RD}\|^2 \right), \quad (2.25)$$

where $\tilde{\mathbf{h}}_{SR}$ is a $(M_R - 1) \times 1$ vector and follows the chi-square distribution with $2(M_R - 1)$ degrees-of-freedom.

2.3.2.4 MRC/MRT Scheme

As another suboptimal approach, principles of MRT and MRC can be employed where \mathbf{w}_r and \mathbf{w}_t are set to match the first hop and second hop channel, respectively. Hence, $\mathbf{w}_r^{\text{MRC}} = \mathbf{h}_{SR}/\|\mathbf{h}_{SR}\|$ and $\mathbf{w}_t^{\text{MRT}} = \mathbf{h}_{RD}^\dagger/\|\mathbf{h}_{RD}\|$. Accordingly, by substituting $\mathbf{w}_r^{\text{MRC}}$ and $\mathbf{w}_t^{\text{MRT}}$ into (2.19), the end-to-end SINR can be expressed as

$$\gamma_{\text{MRC}} = \min \left(c_1 \|\mathbf{h}_{SR}\|^2 \left(\kappa \bar{\gamma}_1 \beta_1 \frac{|\mathbf{h}_{SR}^\dagger \mathbf{H}_{\text{SI}} \mathbf{h}_{RD}^\dagger|^2}{\|\mathbf{h}_{RD}\|^2} + 1 \right)^{-1}, c_2 \|\mathbf{h}_{SR}\|^2 \|\mathbf{h}_{RD}\|^2 \right), \quad (2.26)$$

where $c_1 = \bar{\gamma}_1 \beta_1$ and $c_2 = \kappa \bar{\gamma}_2 \beta_1 \beta_2$. It is worthwhile to note that the optimum, TZF, and RZF schemes reduce to the MRC/MRT scheme in the absence of SI. Although the MRC/MRT scheme is not optimal in the presence of SI, it could be favored in situations where compatibility with HD systems is a concern. Note that the MRC/MRT scheme requires only the knowledge of \mathbf{h}_{SR} and \mathbf{h}_{RD} , whereas the other three schemes require the knowledge of \mathbf{h}_{SR} , \mathbf{h}_{RD} , and \mathbf{H}_{SI} .

2.3.3 Performance Analysis

In this subsection, we evaluate the throughput of the instantaneous transmission and delay-constrained transmission in the cases of optimum and suboptimum schemes.

2.3.3.1 Instantaneous Transmission

The instantaneous throughput of the considered FD wireless-powered relaying system can be computed as [38]

$$R_I(\alpha) = (1 - \alpha) \log_2(1 + \gamma_{\text{FD}}), \quad (2.27)$$

where γ_{FD} (2.19) is a function of α . This expression reveals an interesting trade-off between energy harvesting duration and the instantaneous throughput. A longer energy harvesting time increases the harvested energy and consequently the second hop SNR, however, decreases the available time for information transmission and vice-versa. Therefore, an appropriate system design can optimize the instantaneous throughput by adjusting α . The optimal α is obtained by solving

$$\alpha^* = \arg \max_{0 < \alpha < 1} R_I(\alpha). \quad (2.28)$$

For a given end-to-end SINR or SNR of a particular scheme, $R_I(\alpha)$ in (2.28) is a concave function of α and the optimized α^* can be obtained by solving the

equation $\frac{dR_1(\alpha)}{d\alpha} = 0$. For example, in case of the optimum scheme, by substituting the optimum $\mathbf{w}_t^{\text{OPT}}$, the instantaneous throughput as a function of α is

$$R_1(\alpha) = (1-\alpha) \log_2 \left(1 + \bar{\gamma}_1 \beta_1 \|\mathbf{h}_{SR}\|^2 \min \left(1 - \frac{\alpha b_1}{(1-\alpha) + \alpha b_2}, \frac{\alpha b_0}{1-\alpha} \right) \right), \quad (2.29)$$

where $b_0 = \frac{\bar{\gamma}_2}{\bar{\gamma}_1} \eta \beta_2 \|\mathbf{h}_{RD} \mathbf{w}_t^{\text{OPT}}\|^2$, $b_1 = \eta \bar{\gamma}_1 \beta_1 \|\mathbf{h}_{SR}^\dagger \mathbf{H}_{S1} \mathbf{w}_t^{\text{OPT}}\|^2$, and $b_2 = \eta \bar{\gamma}_1 \beta_1 \|\mathbf{h}_{SR}\|^2 \|\mathbf{H}_{S1} \mathbf{w}_t^{\text{OPT}}\|^2$. The optimization problem (2.28) can be solved by using the procedure described in [44]. Let $a_0 = \eta \bar{\gamma}_2 \beta_1 \beta_2 \|\mathbf{h}_{SR}\|^2 \|\mathbf{h}_{RD} \mathbf{w}_t^{\text{OPT}}\|^2$. Then, the optimal value of α can be obtained as

$$\alpha_{\text{Opt}}^* = \begin{cases} \frac{e^{W\left(\frac{a_0-1}{e}\right)+1} - 1}{a_0 - 1 + e^{W\left(\frac{a_0-1}{e}\right)+1}}, & \text{if } e^{W\left(\frac{a_0-1}{e}\right)+1} < \frac{a_0}{\alpha_0} + 1; \\ \frac{1}{1+\alpha_0}, & \text{otherwise,} \end{cases} \quad (2.30)$$

where $\alpha_0 = \frac{2b_0b_2}{(b_2-b_1-b_0) + \sqrt{b_0^2 + (b_2-b_1)^2 + 2b_0(b_1+b_2)}}$.

Furthermore, optimal α for the proposed suboptimum beamforming schemes can be obtained from (2.30) by replacing a_0 and α_0 from Table 2.2.

An important point to stress is that, in contrast to the suboptimum schemes, the obtained solution of \mathbf{w}_t in the optimum scheme depends on α . As a consequence, joint optimization w.r.t. α and \mathbf{w}_t is required. There are two ways to solve this joint optimization. The first way is to find \mathbf{w}_t by following Proposition 1 and next performing a one-dimensional line search over $0 < \alpha < 1$. This guarantees the global optimum solutions for α and \mathbf{w}_t . Another way is to employ an iterative approach where each iteration step consists of a two-step optimization, i.e., optimizing \mathbf{w}_t for a given α and vice-versa.

Figure 2.5 shows the instantaneous throughput versus the time portion α of the beamforming schemes for an arbitrary frame of block time T . In the simulations, we set the channel variances as $\beta_1 = d_1^{-\nu}$ and $\beta_2 = d_2^{-\nu}$, where d_1 and d_2 denote the distances between the S and R and between R and D , respectively and ν is the path loss exponent. As expected, the optimum scheme outperforms all suboptimum schemes on all TS values. In addition, simulation results, not shown in the figure to avoid clutter, reveal that the values of the optimal α decrease as either the number of

Table 2.2 Suboptimum beamforming schemes' parameters

Scheme	a_0	α_0
TZF	$\eta \bar{\gamma}_2 \beta_1 \beta_2 \ \mathbf{h}_{SR}\ ^2 \ \mathbf{B} \mathbf{h}_{RD}\ ^2$	$\eta \bar{\gamma}_1 \bar{\gamma}_2 \beta_2 \ \mathbf{B} \mathbf{h}_{RD}\ ^2$
RZF	$\eta \bar{\gamma}_2 \beta_1 \beta_2 \ \mathbf{h}_{SR}\ ^2 \ \mathbf{h}_{RD}\ ^2$	$\frac{\bar{\gamma}_2}{\bar{\gamma}_1} \eta \beta_2 \frac{\ \mathbf{h}_{SR}\ ^2 \ \mathbf{h}_{RD}\ ^2}{\ \mathbf{D} \mathbf{h}_{SR}\ ^2}$
MRC/MRT	$\eta \bar{\gamma}_2 \beta_1 \beta_2 \ \mathbf{h}_{SR}\ ^2 \ \mathbf{h}_{RD}\ ^2$	$2\eta \bar{\gamma}_1 \beta_1 \frac{ \mathbf{h}_{SR}^\dagger \mathbf{H}_{S1} \mathbf{h}_{RD}^\dagger ^2}{\ \mathbf{h}_{RD}\ ^2} / \left(\sqrt{1 + \frac{4\beta_1 \bar{\gamma}_1^2}{\beta_2 \bar{\gamma}_2} \frac{ \mathbf{h}_{SR}^\dagger \mathbf{H}_{S1} \mathbf{h}_{RD}^\dagger ^2}{\ \mathbf{h}_{RD}\ ^4}} - 1 \right)$

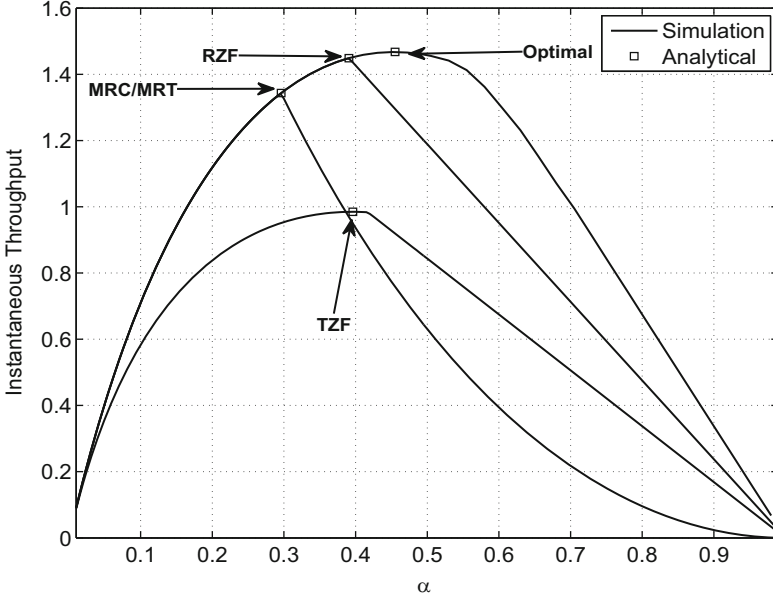


Fig. 2.5 Instantaneous throughput versus α ($M_T = M_R = 3$, $P_S = 20$ dBm, $d_1 = 20$, $d_2 = 10$ and $\nu = 3$)

relays' receive antennas or the sources' transmit power is increased. This is because in these cases the relay node can harvest the same amount of energy in a shorter time. Therefore, more time must be allocated to the information transmission phase in order to improve the throughput.

2.3.3.2 Delay-Constrained Transmission

Throughput of the delay-constrained transmission can be determined by evaluating the outage probability, P_{out} , at a fixed source transmission rate R_c bits/s/Hz where $R_c = \log_2(1 + \gamma_{\text{th}})$ and γ_{th} is the value of SNR for correct data detection at the destination [59]. Due to the time variation of the fading channel, outage events where the instantaneous channel capacity is below the source transmission rate may occur. Therefore, P_{out} can be written as

$$P_{\text{out}} = \Pr(\gamma_{\text{FD}} < \gamma_{\text{th}}) = F_{\gamma_{\text{FD}}}(\gamma_{\text{th}}), \quad (2.31)$$

where $\gamma_{\text{th}} = 2^{R_c} - 1$. Given that the source is communicating R_c bits/sec/Hz and $(1 - \alpha)T$ is the effective communication time from S to D in the block time T seconds, the throughput, $R_D(\alpha)$, in delay-constrained transmission mode is given by [59]

$$R_D(\alpha) = (1 - P_{\text{out}})R_c(1 - \alpha). \quad (2.32)$$

In order to determine the delay-constrained throughput, it is important to characterize the outage probability of each scheme. In the following, both exact and asymptotic expressions for the outage probability of the TZF, RZF, and MRC/MRT schemes are presented. We notice that derivation of the outage probability of the optimum scheme is difficult. Hence we have resorted to simulations for evaluating the delay-constrained throughput of the optimum scheme in Fig. 2.6.

According to (2.23), (2.25), and (2.31), the outage probability at D for TZF and RZF schemes can be expressed as [44]

$$P_{\text{out}}^{\text{TZF}} = 1 - \frac{1}{\Gamma(M_R)} \int_{\frac{\gamma_{\text{th}}}{\gamma_1 \beta_1}}^{\infty} Q\left(M_T - 1, \frac{1}{\kappa \bar{\gamma}_2 \beta_1 \beta_2} \frac{\gamma_{\text{th}}}{x}\right) x^{M_R-1} e^{-x} dx, \quad (2.33)$$

and

$$P_{\text{out}}^{\text{RZF}} = 1 - Q\left(M_R, \frac{\gamma_{\text{th}}}{\gamma_1 \beta_1}\right) + \frac{1}{\Gamma(M_R)} \left(\int_{\frac{\gamma_{\text{th}}}{\gamma_1 \beta_1}}^{\infty} P\left(M_T, \frac{1}{\kappa \bar{\gamma}_2 \beta_1 \beta_2} \frac{\gamma_{\text{th}}}{x}\right) x^{M_R-1} e^{-x} dx \right. \\ \left. + \left(\frac{\gamma_{\text{th}}}{\gamma_1 \beta_1} \right)^{M_R-1} \int_{\frac{\gamma_{\text{th}}}{\gamma_1 \beta_1}}^{\infty} Q\left(M_T, \frac{1}{\kappa \bar{\gamma}_2 \beta_1 \beta_2} \frac{\gamma_{\text{th}}}{x}\right) e^{-x} dx \right), \quad (2.34)$$

respectively, where $Q(a, x) = \Gamma(a, x)/\Gamma(a)$ and $P(a, x) = \gamma(a, x)/\Gamma(a)$.

The outage probability analysis of the MRC/MRT scheme for arbitrary M_T and M_R appears to be cumbersome. Therefore, we only consider two special cases:

- Case (1) $M_T = 1, M_R \geq 1$
- Case (2) $M_T \geq 1, M_R = 1$

Statistics of the associated RVs in both of these special cases can be found. Therefore, using (2.26) and (2.31), outage probability of Cases 1 and 2 can be expressed as [44]

$$P_{\text{out}}^{\text{MRC},1} = 1 - \int_{\frac{\gamma_{\text{th}}}{\gamma_1 \beta_1}}^{\infty} G_{23}^{21} \left(\frac{1}{\kappa \bar{\gamma}_1 \beta_1 \sigma_{\text{SI}}^2} \left(\frac{c_1}{\gamma_{\text{th}}} - \frac{1}{x} \right) \middle| \begin{matrix} 1, M_R \\ 1, M_R, 0 \end{matrix} \right) \frac{x^{M_R-1}}{\Gamma(M_R)} e^{-\left(x + \frac{\gamma_{\text{th}}}{c_2 x}\right)} dx, \quad (2.35)$$

and

$$P_{\text{out}}^{\text{MRC},2} = 1 - \int_{\frac{\gamma_{\text{th}}}{\gamma_1 \beta_1}}^{\infty} \left(1 - e^{-\frac{1}{c_2 x} \left(\frac{c_1 x}{\gamma_{\text{th}}} - 1 \right)} \right) Q\left(M_T, \frac{\gamma_{\text{th}}}{\kappa \bar{\gamma}_1 \beta_1 \sigma_{\text{SI}}^2 x}\right) e^{-x} dx, \quad (2.36)$$

respectively. The integrals in (2.33)–(2.36) do not admit a closed-form solution, however, they can be evaluated numerically. To gain further insights, we now look into the high SNR regime and present simple approximations from [44]. These

expressions enable the characterization of the achievable diversity order of the TZF, RZF, and MRT/MRC schemes.

Proposition 2. *In the high SNR regime, i.e., $\bar{\gamma}_1, \bar{\gamma}_2 \rightarrow \infty$, the outage probability of the TZF scheme can be approximated as: $\mathbf{P}_{\text{out}}^{\text{TZF}} \approx$*

$$\begin{cases} \left(\frac{1}{\Gamma(M_R+1)} + \frac{1}{\Gamma(M_T-1)\Gamma(M_R)} \sum_{k=0}^{\infty} \frac{(-1)^{k+1}}{k!(k+M_T)} \left(\frac{\sigma_D^2}{\sigma_R^2} \frac{1}{\kappa\beta_2} \right)^{M_T+k-1} \frac{1}{M_R-M_T-k+1} \right) \left(\frac{\gamma_{\text{th}}}{\bar{\gamma}_1\beta_1} \right)^{M_R}, & M_T > M_R + 1, \\ \frac{1}{\Gamma(M_R+1)} \left(1 + \frac{1}{\Gamma(M_R)} \left(\ln \left(\frac{\bar{\gamma}_1\beta_1}{\gamma_{\text{th}}} \right) + \psi(1) \right) \left(\frac{\sigma_D^2}{\sigma_R^2} \frac{1}{\kappa\beta_2} \right)^{M_R} \right) \left(\frac{\gamma_{\text{th}}}{\bar{\gamma}_1\beta_1} \right)^{M_R}, & M_T = M_R + 1, \\ \frac{\Gamma(M_R-M_T+1)}{\Gamma(M_T)\Gamma(M_R)} \left(\frac{1}{\kappa\beta_2} \right)^{M_T-1} \left(\frac{\gamma_{\text{th}}}{\bar{\gamma}_2\beta_1} \right)^{M_T-1}, & M_T < M_R + 1. \end{cases} \quad (2.37)$$

By inspecting (2.37), we see that the TZF scheme achieves a diversity order of $\min(M_R, M_T - 1)$. This is intuitive since one degree-of-freedom is used for interference cancellation. Moreover, for the case $M_R + 1 = M_T$, $\mathbf{P}_{\text{out}}^{\text{TZF}}$ decays as $\bar{\gamma}_1^{-M_R} \ln(\bar{\gamma}_1)$ rather than $\bar{\gamma}_1^{-M_R}$ as in the conventional case with fixed power, which implies that in the energy harvesting case the slope of $\mathbf{P}_{\text{out}}^{\text{TZF}}$ converges much slowly.

Proposition 3. *In the high SNR regime, i.e., $\bar{\gamma}_1, \bar{\gamma}_2 \rightarrow \infty$, the outage probability of the RZF scheme can be approximated as*

$$\mathbf{P}_{\text{out}}^{\text{RZF}} \approx \begin{cases} \frac{1}{\Gamma(M_R)} \left(\frac{\gamma_{\text{th}}}{\bar{\gamma}_1\beta_1} \right)^{M_R-1}, & M_R < M_T + 1, \\ \frac{1}{\Gamma(M_R)} \left(1 + \frac{1}{\Gamma(M_T+1)} \left(\frac{\sigma_D^2}{\sigma_R^2} \frac{1}{\kappa\beta_2} \right)^{M_T} \right) \left(\frac{\gamma_{\text{th}}}{\bar{\gamma}_1\beta_1} \right)^{M_T}, & M_R = M_T + 1, \\ \frac{\Gamma(M_R-M_T)}{\Gamma(M_R)\Gamma(M_T+1)} \left(\frac{1}{\kappa\beta_2} \right)^{M_T} \left(\frac{\gamma_{\text{th}}}{\bar{\gamma}_2\beta_1} \right)^{M_T}, & M_R > M_T + 1. \end{cases} \quad (2.38)$$

Proposition 3 indicates that the RZF scheme achieves a diversity order of $\min(M_R - 1, M_T)$. This result is also intuitively satisfying since one degree-of-freedom should be allocated for SI cancellation at the receive side of R.

Proposition 4. *In the high SNR regime, i.e., $\bar{\gamma}_1, \bar{\gamma}_2 \rightarrow \infty$, with $M_T = 1$ the outage probability of the MRC/MRT scheme can be approximated as*

$$\mathbf{P}_{\text{out}}^{\text{MRC},1} \approx 1 - \frac{2}{\Gamma(M_R)} G_{23}^{21} \left(\frac{1}{\kappa\sigma_{\text{SI}}^2\gamma_{\text{th}}} \middle| \begin{matrix} 1, M_R \\ 1, M_R, 0 \end{matrix} \right) \left(\frac{\gamma_{\text{th}}}{\kappa\bar{\gamma}_2\beta_1\beta_2} \right)^{\frac{M_R}{2}} K_{M_R} \left(2\sqrt{\frac{\gamma_{\text{th}}}{\kappa\bar{\gamma}_2\beta_1\beta_2}} \right). \quad (2.39)$$

Moreover, by applying a Bessel function approximation for small arguments, $K_\nu(x) \approx \frac{\Gamma(\nu)}{2} \left(\frac{x}{2} \right)^{-\nu}$, in (2.39) we can write

$$\mathbf{P}_{\text{out}}^{\text{MRC},1} \rightarrow 1 - G_{23}^{21} \left(\frac{1}{\kappa \sigma_{\text{SI}}^2 \gamma_{\text{th}}} \mid \begin{matrix} 1, M_R \\ 1, M_R, 0 \end{matrix} \right). \quad (2.40)$$

Note that (2.40) presents the outage probability floor and indicates that the MRC/MRT scheme with $M_T = 1$ exhibits a zero-diversity order in presence of residual SI.

Proposition 5. *In the high SNR regime, i.e., $\bar{\gamma}_1, \bar{\gamma}_2 \rightarrow \infty$, with $M_R = 1$, the outage probability of the MRC/MRT scheme can be approximated as*

$$\begin{aligned} \mathbf{P}_{\text{out}}^{\text{MRC},2} \approx & 1 - \left(1 - e^{-\frac{1}{\kappa \sigma_{\text{SI}}^2 \gamma_{\text{th}}}} \right) \left(e^{-\frac{\gamma_{\text{th}}}{\bar{\gamma}_1 \beta_1}} - \frac{\gamma_{\text{th}}}{\bar{\gamma}_1 \beta_1 \Gamma(M_T)} \sum_{k=0}^{\infty} \frac{(-1)^k}{k! (M_T + k)} \right. \\ & \times \left. \left(\frac{\bar{\gamma}_1}{\bar{\gamma}_2} \frac{1}{\kappa \beta_2} \right)^{M_T + k} E_{M_T + k} \left(\frac{\gamma_{\text{th}}}{\bar{\gamma}_1 \beta_1} \right) \right). \end{aligned} \quad (2.41)$$

At this point, it is important to determine the value of α that maximizes the throughput. We note that delay-constrained throughput should converge to the ceiling value of $R_c(1 - \alpha)$ when $\mathbf{P}_{\text{out}} \rightarrow 0$. For each beamforming scheme we observe that \mathbf{P}_{out} is a complicated function of α and it decreases as the value of α is increased. However, this will lead to the decrease of the term $(1 - \alpha)$ at the same time. Therefore, an optimal value of α that maximizes the delay-constrained throughput exists and it can be found by solving the following optimization problem:

$$\alpha^* = \arg \max_{0 < \alpha < 1} R_D(\alpha). \quad (2.42)$$

Given (2.33)–(2.36), the optimization problem in (2.42) does not admit closed-form solutions. However, the optimal α^* can be solved numerically. Figure 2.6 demonstrates the impact of optimal α on the delay-constrained throughput. The superior performance of the optimum scheme compared to suboptimal schemes is more pronounced especially between 0.4 and 0.8 values of α . The highest throughput with optimized α for the optimum, RZF, MRC/MRT, and TZF schemes are given by 0.6517, 0.6396, 0.5672, and 0.4824, respectively. Moreover, we see that each one of the TZF, RZF, and MRC/MRT schemes can surpass other schemes depending on the value of α . This observation reveals the existence of various design choices when performance-complexity trade-off becomes a design factor. It is also observed that all schemes achieve significant throughput gains as compared to the HD mode.

Simulations also show that as long as a beamforming scheme is capable of cancelling the SI, the delay-constrained throughput can be improved as either the number of relays' receive antennas or the sources' transmit power is increased. This is because, the amount of the harvested energy at the relay is increased and consequently the outage probability is decreased, i.e., $\mathbf{P}_{\text{out}} \rightarrow 0$. Therefore, the delay-constrained throughput tends to $R_D(\alpha) \rightarrow R_c(1 - \alpha)$ which approximately

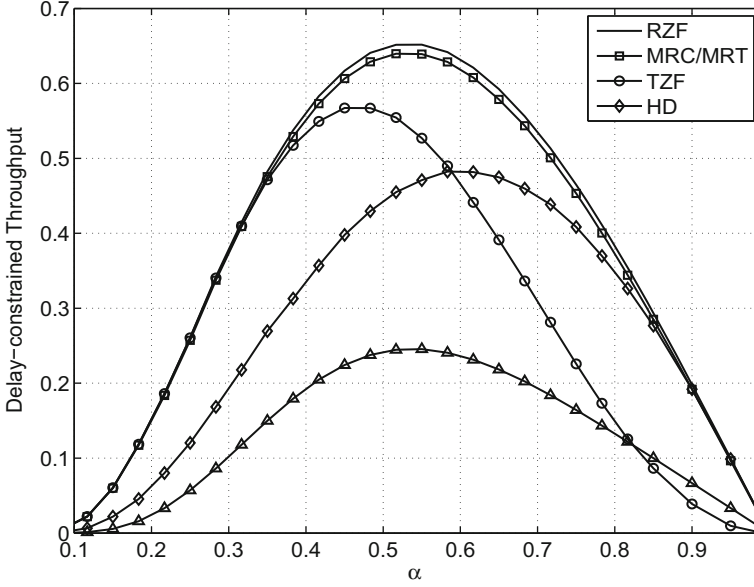


Fig. 2.6 Delay-constrained throughput of different schemes ($M_T = M_R = 3$, $P_S = 10$ dBm, $d_1 = 15$, $d_2 = 10$, $\eta = 0.5$, and $R_c = 2$)

deliver the highest throughput for some small values of the α . However, an excessive amount of harvested energy at R is not always advantageous. For example, in case of MRC/MRT scheme it is detrimental since it results in a strong irreducible SI effect at R .

2.4 Full-Duplex Information and Power Transfer with Hybrid AP

If a BS or an AP is empowered with FD operation, simultaneous uplink and downlink transmission among a set of users can be implemented. Thus, in addition to FD bi-directional and relay topologies, some papers have also considered the above scenario [45, 46, 60]. The gains that can be achieved with the help of the FD BS (or AP) topology are largely influenced by the residual SI at the BS (or AP) as well as the inter-user interference at downlink users due to uplink user transmissions. Moreover in multi-cell environments, compared to HD operation that employs time-division duplexing (TDD) or frequency-division duplexing, simultaneous uplink and downlink transmissions can cause different interference patterns [61]. Hence, in order to reap the spectral efficiency gains promised by the FD mode, systems based on the BS topology need to be carefully designed [62].

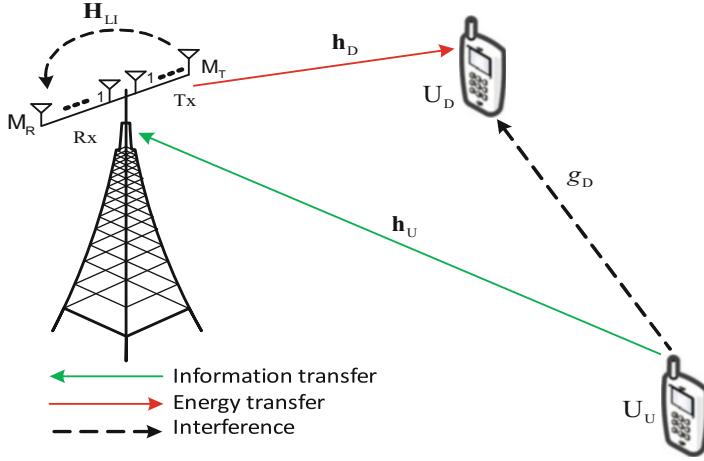


Fig. 2.7 FD hybrid data-and-energy transfer system

In the sequel, a design to maximize the rate-energy region of a FD system with one multi-antenna hybrid AP, one uplink user, and one energy harvester downlink user is presented.

2.4.1 System Model

Consider a FD system, as shown in Fig. 2.7, consisting of a hybrid AP, one uplink user (\$U_U\$), and one downlink user (\$U_D\$). Both \$U_U\$ and \$U_D\$ are equipped with a single antenna, while the AP is equipped with \$M_R\$ receive antennas and \$M_T\$ transmit antennas. The FD AP communicates with \$U_U\$ in the uplink and transmits energy to \$U_D\$ in the downlink at the same time over the same frequency band [45, 46]. Denote \$\mathbf{h}_U \in \mathbb{C}^{M_R \times 1}\$ as the channel vector from the \$U_U\$ to AP, \$\mathbf{h}_D \in \mathbb{C}^{M_T \times 1}\$ as the channel vector from AP to the \$U_D\$, \$\mathbf{H}_{SI} \in \mathbb{C}^{M_R \times M_T}\$ as the residual SI channel from transmit antennas to the receive antennas at FD AP, and \$g_D\$ as the channel coefficient from \$U_U\$ to \$U_D\$. The transmit and receive beamformers at the AP are \$\mathbf{w}_t\$ and \$\mathbf{w}_r\$, respectively.

Given the total transmit power \$P_{AP}\$ at the AP, the harvested energy at the \$U_D\$ is \$E = \eta (P_{AP} |\mathbf{h}_D^\dagger \mathbf{w}_t|^2 + P_U |g_D|^2)\$ where \$P_U\$ is the transmit power of \$U_U\$. Moreover, SINR at the FD AP can be expressed as

$$\gamma_U = \frac{P_U |\mathbf{w}_r^\dagger \mathbf{h}_U|^2}{P_{AP} |\mathbf{w}_r^\dagger \mathbf{H}_{SI} \mathbf{w}_t|^2 + \|\mathbf{w}_r\|^2 \sigma_n^2}, \quad (2.43)$$

where \$\sigma_n^2\$ is the noise power at the AP.

Our objective is to maximize the uplink rate of U_U by jointly designing the transmit and receive beamformers at the AP, subject to an EH constraints. Thus, the following optimization problem is formulated as:

$$\begin{aligned} \max_{\|\mathbf{w}_r\|=\|\mathbf{w}_t\|=1} \quad & R_U = \log_2 \left(1 + \frac{P_U |\mathbf{w}_r^\dagger \mathbf{h}_U|^2}{P_{AP} |\mathbf{w}_r^\dagger \mathbf{H}_{SI} \mathbf{w}_t|^2 + \sigma_n^2} \right), \\ \text{s.t.} \quad & \eta \left(P_{AP} |\mathbf{h}_D^\dagger \mathbf{w}_t|^2 + P_U |g_D|^2 \right) \geq \bar{E}, \end{aligned} \quad (2.44)$$

where \bar{E} denotes the minimum requirement of the harvested energy at the U_D .

2.4.2 Precoding Design for Rate-Energy Maximization

The joint optimization problem (2.44) can be solved by first optimizing over \mathbf{w}_r while fixing \mathbf{w}_t . For a given \mathbf{w}_t that satisfies the constraint in (2.44), the optimization problem w.r.t. \mathbf{w}_r reduces to

$$f_{re} \triangleq \max_{\|\mathbf{w}_r\|=1} \frac{P_U |\mathbf{w}_r^\dagger \mathbf{h}_U|^2}{P_{AP} |\mathbf{w}_r^\dagger \mathbf{H}_{SI} \mathbf{w}_t|^2 + \sigma_n^2}. \quad (2.45)$$

Define $\bar{\mathbf{A}} \triangleq [P_{AP} \mathbf{H}_{SI} \mathbf{w}_t \mathbf{w}_t^\dagger \mathbf{H}_{SI}^\dagger + \sigma_n^2 \mathbf{I}]$. The optimum \mathbf{w}_r is given by

$$\mathbf{w}_r = \frac{\bar{\mathbf{A}}^{-1} \mathbf{h}_U}{\|\bar{\mathbf{A}}^{-1} \mathbf{h}_U\|}. \quad (2.46)$$

Substitution of \mathbf{w}_r from (2.46) into (2.45) yields

$$\begin{aligned} f_{re} &= P_U \mathbf{h}_U^\dagger [P_{AP} \mathbf{H}_{SI} \mathbf{w}_t \mathbf{w}_t^\dagger \mathbf{H}_{SI}^\dagger + \sigma_n^2 \mathbf{I}]^{-1} \mathbf{h}_U \\ &= \frac{P_U}{\sigma_n^2} \left[\|\mathbf{h}_U\|^2 - \frac{P_{AP} \mathbf{h}_U^\dagger \mathbf{H}_{SI} \mathbf{w}_t \mathbf{w}_t^\dagger \mathbf{H}_{SI}^\dagger \mathbf{h}_U}{\sigma_n^2 + P_{AP} \mathbf{w}_t^\dagger \mathbf{H}_{SI}^\dagger \mathbf{H}_{SI} \mathbf{w}_t} \right], \end{aligned} \quad (2.47)$$

where the second expression is due to the application of Sherman–Morrison formula [30]. Consequently, the joint optimization (2.44) reduces to an optimization problem over \mathbf{w}_t , which is expressed as

$$\begin{aligned} \max_{\|\mathbf{w}_t\|=1} \quad & \log_2 (1 + f_{re}) \\ \text{s.t.} \quad & \eta \left(P_{AP} |\mathbf{h}_D^\dagger \mathbf{w}_t|^2 + P_U |g_D|^2 \right) \geq \bar{E}, \end{aligned} \quad (2.48)$$

which is equivalent to

$$\begin{aligned} \min_{\|\mathbf{w}_t\|=1} \quad & \frac{\mathbf{h}_U^\dagger \mathbf{H}_{\text{SI}} \mathbf{w}_t \mathbf{w}_t^\dagger \mathbf{H}_{\text{SI}}^\dagger \mathbf{h}_U}{\sigma_n^2 + P_{\text{AP}} \mathbf{w}_t^\dagger \mathbf{H}_{\text{SI}}^\dagger \mathbf{H}_{\text{SI}} \mathbf{w}_t} \\ \text{s.t.} \quad & |\mathbf{h}_D^\dagger \mathbf{w}_t|^2 \geq \frac{1}{P_{\text{AP}}} \left[\frac{\bar{E}}{\eta} - P_U |g_D|^2 \right]. \end{aligned} \quad (2.49)$$

The optimization problem (2.49) does not admit a closed-form solution for the optimum \mathbf{w}_t . Its numerical solution is attainable, however, (2.49) is not a convex problem. Introducing an auxiliary variable τ , a matrix variable $\mathbf{W}_t = \mathbf{w}_t \mathbf{w}_t^\dagger$, and relaxing the non-convex rank-one constraint on \mathbf{W}_t , (2.49) can be expressed as an SDR problem

$$\begin{aligned} \min_{\mathbf{W}_t, \tau} \quad & \tau \\ \text{s.t.} \quad & \text{tr} \left(\mathbf{W}_t \left(\tau \left(\sigma_n^2 \mathbf{I} + \mathbf{H}_{\text{SI}} \mathbf{H}_{\text{SI}}^\dagger \right) - \mathbf{H}_{\text{SI}}^\dagger \mathbf{h}_U \mathbf{h}_U^\dagger \mathbf{H}_{\text{SI}} \right) \right) \geq 0, \\ & \text{tr} \left(\mathbf{W}_t \mathbf{h}_D \mathbf{h}_D^\dagger \right) \geq \bar{c}, \\ & \text{tr}(\mathbf{W}_t) = 1, \mathbf{W}_t \succeq 0, \end{aligned} \quad (2.50)$$

where $\bar{c} = \frac{1}{P_{\text{AP}}} \left[\frac{\bar{E}}{\eta} - P_U |g_D|^2 \right]$. Let \mathbf{W}_t^* be an optimum solution in (2.49) for a given τ . Using similar arguments as in the case of (2.7), it can be shown that \mathbf{W}_t^* is rank-one. The optimization (w.r.t. \mathbf{W}_t) has to be solved for all possible values of τ , where $\tau \in [0, \tau_{\max}]$, i.e., a grid search over τ is required.¹ However, the computational cost of solving (2.49) can be significantly reduced by solving it as a feasibility problem. In particular, it is clear that the minimum τ is the one for which the optimization problem (2.49) turns to be feasible. As such, the joint optimum solutions of τ and \mathbf{W}_t can be determined using the following steps:

1. Define a fine grid of τ in steps of $\partial\tau$,
2. Solve (2.49) with the smallest τ , i.e., $\tau = 0$,
3. If feasible, stop and output τ and \mathbf{W}_t ,
4. If not, repeat step (2) with the increment of $\partial\tau$.

As soon as the problem is feasible, the above iterative approach can be stopped and the optimum \mathbf{w}_t is recovered from the eigenvalue decomposition of \mathbf{W}_t . In particular, since the optimum happens to be \mathbf{W}_t rank-one, \mathbf{w}_t is the eigenvector corresponding to the largest eigenvalue (also the only one non-zero eigenvalue) of \mathbf{W}_t .

¹Although τ_{\max} can be analytically calculated, it is not required for solving (2.49).

In order to understand the gains of FD operation, a common practice adopted in the literature is to compare with HD mode. We compare the performance of FD and HD modes of operation at the hybrid AP under the so-called RF chain preserved condition.² In the HD mode of AP operation, hybrid AP employs orthogonal time slots to serve the uplink and downlink users. At the uplink we use MRC to combine the received signals and deploy MRT as the beamformer to transmit energy towards the downlink user. Without loss of any generality, we normalize T to 1 and devote $0 < \alpha^{\text{HD}} \leq 1$ fraction of the block time for energy transfer and $(1 - \alpha^{\text{HD}})$ for information transfer. For a fair comparison, the EH constraint of the downlink user in the HD mode is set as the harvested energy in the FD mode. Therefore, $\alpha^{\text{HD}} = \frac{E}{\eta P_{\text{AP}} \|\mathbf{h}_{\text{D}}\|^2}$ and $R_{\text{U}}^{\text{HD}} = (1 - \alpha^{\text{HD}}) \log_2 (1 + P_{\text{U}} \|\mathbf{h}_{\text{U}}\|^2 / \sigma_n^2)$.

Figure 2.8 shows rate-energy region with $M_R = 2$ and $M_T = 5$, when $P_{\text{U}} = 10$ dBm, $P_{\text{AP}} = 40$ dBm, and $\eta = 0.7$. We consider a scenario where a line-of-sight (LoS) link is present between the AP and the downlink user and for which the complex channel gain vector from the AP to downlink user can be represented by the Rician fading model as [63]

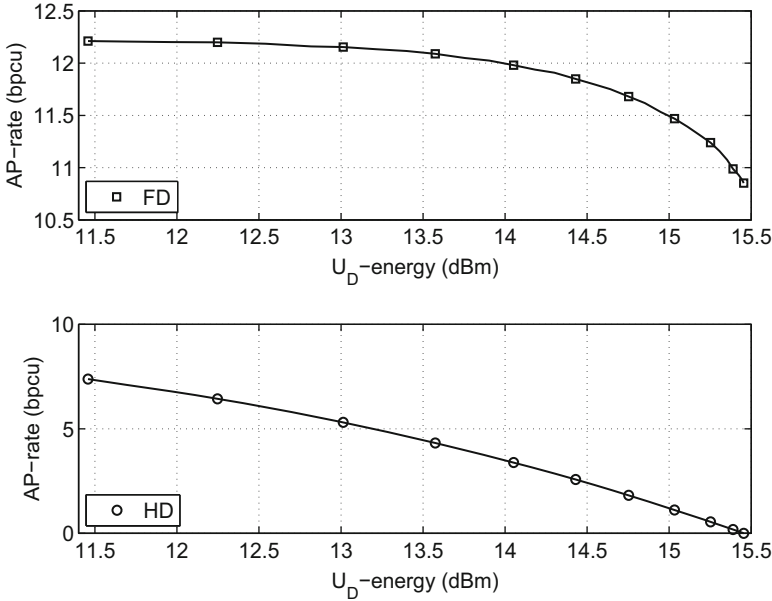


Fig. 2.8 Comparison of rate-energy regions with $M_R = 2$ and $M_T = 5$

²RF chains have a higher cost than antenna elements and therefore FD/HD studies based on RF chain preserved condition as compared to “antenna-preserved” condition have been widely used in the literature for fair comparison.

$$\mathbf{h}_D = \sqrt{\frac{\beta K}{K+1}} \mathbf{h}_{D,d} + \sqrt{\frac{\beta}{K+1}} \mathbf{h}_{D,s}, \quad (2.51)$$

where $\mathbf{h}_{D,d}$ represents the LoS component, β denotes path loss effect, K is the Rician K -factor, and $\mathbf{h}_{D,s}$ denotes the scattered components of the channel. Furthermore, we utilize the far-field uniform linear antenna array model as in [63].

The EH constraint is varied from 0 dBm to \bar{E}^{\max} which is obtained by applying MRT beamformer at the AP. We also assume that the distance between the AP and U_D is 10 meters and $K = 5$ dB. The curves in Fig. 2.8 show that the FD mode of operation can provide significant performance gains. For example, FD AP can provide a higher uplink rate as compared to the HD mode in all regions of the harvested energy. Moreover, the decrease in the uplink rate when the harvested energy varies from the minimum value to the maximum is more in HD. Under HD operation, the downlink user does not exploit the inter-user interference for energy harvesting, a high value of α^{HD} causes the uplink rate to be reduced.

2.5 Future Directions

Research community faces a number of challenges ahead for the design and deployment of FD wireless-powered systems. From a practical perspective these challenges can be categorized into several key areas as outlined below:

- **Full-duplex transceiver design:** Research on SI cancellation algorithm development is required to guarantee practical FD transceiver implementation with flexible energy harvesting capability. Research on SI mitigation techniques with low energy consumption is crucial since circuitry required in the cancellation step could drain harvested energy significantly. Further, nonlinear behavior of the energy harvesting circuit components needs to be captured accurately via new mathematical modeling. Such advances will offer new opportunities for system optimization. In order to test transceiver solutions, test-bed development needs to be undertaken as well.
- **Interference exploitation:** Traditionally in wireless system design, interference has been considered as a detrimental factor. However, in energy harvesting communications, interference can be exploited as an extra source of energy. A FD BS can simultaneously schedule the uplink and downlink transmission on the same resource block, and hence as compared to traditional HD systems, high interference conditions within the cell and from neighboring cells can be expected [62]. As of now, how such interference can be best exploited to improve the performance of FD wireless-powered systems is unknown. Therefore, it is worthwhile to conduct research on transmission schemes, scheduling and interference cancellation algorithms that can strike a good balance between harvested energy and performance.

- **MIMO implementation:** In the context of FD wireless-powered systems, MIMO techniques can be used for spatial-domain SI cancellation and to harvest more energy. However, often optimal solutions that maximize the rate-energy trade-off in FD wireless-powered systems are complex and require significant energy consumption for computation purposes. Hence, it is worth looking at low-complexity MIMO schemes suitable for efficient FD MIMO design. As an example, flexible and low-complexity MIMO architectures that dynamically adapt to the energy harvesting environment and assign different number of antennas for energy harvesting/information transfer seem an interesting direction to pursue.
- **MAC layer design:** While majority of research on FD so far have considered physical layer aspects, research work on MAC layer issues has been still on infancy. In particular, MAC layer operations from an energy consumption point are less understood. Significant research efforts must be dedicated to model FD MAC layer behavior and propose algorithms that can operate with minimum energy. Moreover, whenever possible, the design of cross-layer algorithms that can exploit information available at physical, MAC, and network layer should be promoted [64].
- **Co-existence issues with HD systems:** FD mode is capable of providing performance gains in terms of the throughput over HD mode in several cases. However, in other cases, such as under asymmetric traffic scenarios and high SNR conditions, HD mode outperforms the FD mode. Several works have already proposed hybrid schemes, where the system could operate either in HD mode or FD mode. Advantages of switching between HD/FD in the context of wireless-powered communications are not well understood at present and investigations must be carried out to find whether such hybrid operation would be beneficial. In addition, future wireless networks will be mainly heterogeneous and both HD and FD nodes would operate. From a network perspective, the presence of HD nodes will create new opportunities for the efficient design of future FD wireless-powered systems.

2.6 Conclusions

In this chapter, we considered the application of FD in WPCNs under bi-directional, relay, and hybrid AP topologies. We first considered an N -antenna BS and a wireless-powered MS and characterized optimum and suboptimum schemes for optimizing bi-directional information rates between the BS and MS. The beam-former at the BS and the TS parameter was jointly optimized for both optimum and suboptimum schemes. Compared to the HD operation, a significant improvement in the BS-MS rate region can be observed. Then, we studied the instantaneous and delay-constrained throughput of a FD wireless-powered MIMO relay system. We considered optimum linear processing at the relay as well as several suboptimum schemes. Next, optimum transceiver design for SWIPT in a FD system with one

hybrid AP, one downlink energy user, and one uplink user was investigated. We jointly optimized the transmit and receiver beamformers at the AP to maximize the uplink rate subject to EH constraint at the downlink user. We showed how transmit and receiver beamformers at the AP, that maximize the uplink rate subject to EH constraint at the downlink user, can be designed. In all cases, results that are useful for evaluating the performance and extracting insights into the effects of key parameters, such as the antenna configuration, linear processing scheme, and TS parameters, on the performance were presented. In certain regimes, FD mode shows a better throughput as compared to the HD mode. Therefore, FD operation is a promising approach to design energy and spectrally efficient future wireless communication networks.

References

1. A. Sabharwal, P. Schniter, D. Guo, D.W. Bliss, S. Rangarajan, R. Wichman, In-band full-duplex wireless: challenges and opportunities. *IEEE J. Sel. Areas Commun.* **32**(9), 1637–1652 (2014)
2. Z. Zhang, K. Long, A.V. Vasilakos, L. Hanzo, Full-duplex wireless communications: challenges, solutions, and future research directions. *Proc. IEEE* **104**(7), 1369–1409 (2016)
3. J.I. Choi, M. Jain, K. Srinivasan, P. Levis, S. Katti, Achieving single channel, full duplex wireless communication, in *Proceedings of 16th International Conference on Mobile Computing and Networking (MobiCom'10)*, Chicago, IL, September (2010), pp. 1–12
4. M. Duarte, C. Dick, A. Sabharwal, Experiment-driven characterization of full-duplex wireless systems. *IEEE Trans. Wirel. Commun.* **11**(12), 4296–4307 (2012)
5. E. Aryafar, M.A. Khojastepour, K. Sundaresan, S. Rangarajan, M. Chiang, MIDU: enabling MIMO full duplex, in *Proceedings of 18th International Conference on Mobile Computing and Networking (MobiCom'12)*, New York, August (2012), pp. 257–268
6. T. Riihonen, S. Werner, R. Wichman, Hybrid full-duplex/half-duplex relaying with transmit power adaptation. *IEEE Trans. Wirel. Commun.* **10**(9), 3074–3085 (2011)
7. T. Riihonen, S. Werner, R. Wichman, Mitigation of loopback self-interference in full-duplex MIMO relays. *IEEE Trans. Signal Process.* **59**(12), 5983–5993 (2011)
8. S.S. Hong, J. Brand, J.I. Choi, M. Jain, J. Mehlman, S. Katti, P. Levis, Applications of self-interference cancellation in 5G and beyond. *IEEE Commun. Mag.* **52**(2), 114–121 (2014)
9. E. Everett, A. Sahai, A. Sabharwal, Passive self-interference suppression for full-duplex infrastructure nodes. *IEEE Trans. Wirel. Commun.* **13**(2), 680–694 (2014)
10. M. Heino, D. Korpi, T. Huusari, E. Antonio-Rodriguez, S. Venkatasubramanian, T. Riihonen, L. Anttila, C. Icheln, K. Haneda, R. Wichman, M. Valkama, Recent advances in antenna design and interference cancellation algorithms for in-band full duplex relays. *IEEE Commun. Mag.* **53**(5), 91–101 (2015)
11. European FP7 project DUPLO (full-duplex radios for local access) European commission - research: the seventh framework programme [Online]. Technical Report (2012). Available: <http://www.fp7-duplo.eu/index.php/general-info>
12. T. Riihonen, R. Wichman, Energy detection in full-duplex cognitive radios under residual self-interference, in *Proceedings of International Conference on Cognitive Radio Oriented Wireless Networks and Communications (CrownCom'14)*, Oulu, June (2014), pp. 57–60
13. G. Zheng, I. Krikidis, I. Li, A.P. Petropulu, B.E. Ottersten, Improving physical layer secrecy using full-duplex jamming receivers. *IEEE Trans. Signal Process.* **61**(20), 4962–4974 (2013)
14. S. Priya, D.J. Inman, *Energy Harvesting Technologies* (Springer, Boston, MA, 2009)
15. X. Lu, P. Wang, D. Niyato, D.I. Kim, Z. Han, Wireless networks with RF energy harvesting: a contemporary survey. *IEEE Commun. Surv. Tut.* **17**(2), 757–789 (2015, Second quarter)

16. S. Ulukus, A. Yener, E. Erkip, O. Simeone, M. Zorzi, P. Grover, K. Huang, Energy harvesting wireless communications: a review of recent advances, *IEEE J. Sel. Areas Commun.* **33**(3), 360–381 (2015)
17. K. Huang, V.K.N. Lau, Enabling wireless power transfer in cellular networks: architecture, modeling and deployment. *IEEE Trans. Wirel. Commun.* **13**(2), 902–912 (2014)
18. S. Bi, C.K. Ho, R. Zhang, Wireless powered communication: opportunities and challenges. *IEEE Commun. Mag.* **53**(4), 117–125 (2015)
19. R. Zhang, C.K. Ho, MIMO broadcasting for simultaneous wireless information and power transfer. *IEEE Trans. Wirel. Commun.* **12**(5), 1989–2001 (2013)
20. K.J. Lee, H.B. Kong, H. Lee, S.R. Lee, I. Lee, Optimal beamforming designs for wireless information and power transfer in MISO interference channels. *IEEE Trans. Wirel. Commun.* **14**(9), 4810–4821 (2015)
21. E.S. Lo, D.W.K. Ng, R. Schober, Wireless information and power transfer: energy efficiency optimization in OFDMA systems. *IEEE Trans. Wirel. Commun.* **12**(12), 6352–6370 (2013)
22. H. Tabassum, E. Hossain, On the deployment of energy sources in wireless-powered cellular networks. *IEEE Trans. Commun.* **63**(9), 3391–3404 (2015)
23. B. Clerckx, E. Bayguzina, Waveform design for wireless power transfer. *IEEE Trans. Signal Process.* **64**(23), 6313–6328 (2016)
24. S. O'Driscoll, A.S.Y. Poon, T.H. Meng, Optimal frequency for wireless power transmission into dispersive tissue. *IEEE Trans. Antennas Propag.* **58**(5), 1739–1750 (2010)
25. W.C. Brown, The history of power transmission by radio waves. *IEEE Trans. Microwave Theory Tech.* **32**(9), 1230–1242 (1984)
26. L.R. Varshney, Transporting information and energy simultaneously, in *Proceedings of IEEE International Symposium on Information Theory (ISIT 2008)*, Toronto July (2008), pp. 1612–1616
27. Z. Ding, C. Zhong, D.W.K. Ng, M. Peng, H.A. Suraweera, R. Schober, H.V. Poor, Application of smart antenna technologies in simultaneous wireless information and power transfer. *IEEE Commun. Mag.* **53**(4), 86–93 (2015)
28. Y. Zeng, R. Zhang, Full-duplex wireless-powered relay with self-energy recycling. *IEEE Wirel. Commun. Lett.* **4**(2), 201–204 (2015)
29. M. Maso, C. Liu, C. Lee, T.Q.S. Quek, L.S. Cardoso, Energy-recycling full-duplex radios for next-generation networks. *IEEE J. Sel. Areas Commun.* **33**(12), 2948–2962 (2015)
30. M. Mohammadi, H.A. Suraweera, Y. Cao, I. Krikidis, C. Tellambura, Full-duplex radio for uplink/downlink wireless access with spatially random nodes. *IEEE Trans. Commun.* **63**(12), 5250–5266 (2015)
31. S. Goyal, C. Galiotto, N. Marchetti, S.S. Panwar, Throughput and coverage for a mixed full and half duplex small cell network, in *Proceedings of IEEE International Conference on Communications (ICC'16)*, Kuala Lumpur, May (2016), pp. 1–7
32. Y.L. Che, J. Xu, L. Duan, R. Zhang, Multiantenna wireless powered communication with cochannel energy and information transfer. *IEEE Commun. Lett.* **19**(12), 2266–2269 (2015)
33. Z. Hu, C. Yuan, F. Zhu, F. Gao, Weighted sum transmit power minimization for full-duplex system with SWIPT and self-energy recycling. *IEEE Access.* **4**, 4874–4881 (2016)
34. M. Gao, H.H. Chen, Y. Li, M. Shirvanimoghaddam, J. Shi, Full-duplex wireless-powered communication with antenna pair selection, in *Proceedings of IEEE Wireless Communications and Networking Conference (WCNC'15)*, New Orleans, LA, March (2015), pp. 693–698
35. A.A. Okandjei, M.R.A. Khandaker, K. Wong, Wireless information and power transfer in full-duplex communication systems, in *Proceedings of IEEE International Conference on Communications (ICC'16)*, Kuala Lumpur, May (2016), pp. 1–6
36. W. Mou, Y. Cai, W. Yang, W. Yang, X. Xu, J. Hu, Exploiting full duplex techniques for secure communication in SWIPT system, in *Proceedings of International Conference on Wireless Communications and Signal Processing (WCSP'15)*, Nanjing, October (2015), pp. 1–6
37. Y. Xiao, Z. Xiong, D. Niyato, Z. Han, L.A. DaSilva, Full-duplex machine-to-machine communication for wireless-powered internet-of-things, in *Proceedings of IEEE International Conference on Communications (ICC'16)*, Kuala Lumpur, May (2016), pp. 1–6

38. C. Zhong, H.A. Suraweera, G. Zheng, I. Krikidis, Z. Zhang, Wireless information and power transfer with full duplex relaying. *IEEE Trans. Commun.* **62**(10), 3447–3461 (2014)
39. S. Hu, Z. Ding, Q. Ni, Beamforming optimisation in energy harvesting cooperative full-duplex networks with self-energy recycling protocol. *IET Commun.* **10**(7), 848–853 (2016)
40. Z. Wen, X. Liu, N.C. Beaulieu, R. Wang, S. Wang, Joint source and relay beamforming design for full-duplex MIMO AF relay SWIPT systems. *IEEE Commun. Lett.* **20**(2), 320–323 (2016)
41. I. Krikidis, G. Zheng, B.E. Ottersten, Harvest-use cooperative networks with half/full-duplex relaying, in *Proceedings of IEEE Wireless Communications and Networking Conference (WCNC'13)*, Shanghai, April (2013), pp. 4256–4260
42. H. Liu, K.J. Kim, K.S. Kwak, H.V. Poor, Power splitting-based SWIPT with decode-and-forward full-duplex relaying. *IEEE Trans. Wirel. Commun.* **15**(11), 7561–7577 (2016)
43. T. Riihonen, L. Zhao, M. Vehkaperä, X. Wang, On the feasibility of full-duplex relaying powered by wireless energy transfer, in *Proceedings of IEEE Workshop on Signal Processing Advances in Wireless Communications (SPAWC'16)*, Edinburgh, July (2016), pp. 1–5
44. M. Mohammadi, B.K. Chalise, H.A. Suraweera, C. Zhong, G. Zheng, I. Krikidis, Throughput analysis and optimization of wireless-powered multiple antenna full-duplex relay systems. *IEEE Trans. Commun.* **64**(4), 1769–1785 (2016)
45. H. Ju, R. Zhang, Optimal resource allocation in full-duplex wireless-powered communication network. *IEEE Trans. Commun.* **62**(10), 3528–3540 (2014)
46. X. Kang, C.K. Ho, S. Sun, Full-duplex wireless-powered communication network with energy causality. *IEEE Trans. Wirel. Commun.* **14**(10), 5539–5551 (2015)
47. H. Kim, H. Lee, M. Ahn, H. Kong, I. Lee, Joint subcarrier and power allocation methods in full duplex wireless powered communication networks for OFDM systems. *IEEE Trans. Wirel. Commun.* **15**(7), 4745–4753 (2016)
48. S. Leng, D.W.K. Ng, N. Zlatanov, R. Schober, Multi-objective resource allocation in full-duplex SWIPT systems, in *Proceedings of IEEE International Conference on Communications (ICC'16)*, Kuala Lumpur, May (2016), pp. 1–7
49. V.-D. Nguyen, H.V. Nguyen, G.-M. Kang, H.M. Kim, O.-S. Shin, Sum rate maximization for full duplex wireless-powered communication networks, in *Proceedings of European Signal Processing Conference (EUSIPCO'16)*, Budapest (2016), pp. 798–802
50. Y. Wang, R. Sun, X. Wang, Transceiver design to maximize the weighted sum secrecy rate in full-duplex SWIPT systems. *IEEE Signal Process. Lett.* **23**(6), 883–887 (2016)
51. K. Yamazaki, Y. Sugiyama, Y. Kawahara, S. Saruwatari, T. Watanabe, Preliminary evaluation of simultaneous data and power transmission in the same frequency channel, in *Proceedings of IEEE Wireless Communications and Networking Conference (WCNC'15)*, New Orleans, LA, March (2015), pp. 1237–1242
52. R.M. Corless, G.H. Gonnet, D.E.G. Hare, D.J. Jeffrey, D.E. Knuth, On the Lambert W function. *Adv. Comput. Math.* **5**(4), 329–359 (1996)
53. I.S. Gradshteyn, I.M. Ryzhik, *Table of Integrals, Series and Products*, 7th edn. (Academic, San Diego, CA, 2007)
54. B.K. Chalise, H.A. Suraweera, G. Zheng, Throughput maximization for full-duplex energy harvesting MIMO communications, in *Proceedings of IEEE Workshop on Signal Processing Advances in Wireless Communications (SPAWC'16)*, Edinburgh, July (2016), pp. 1–5
55. B.K. Chalise, W. Ma, Y.D. Zhang, H.A. Suraweera, M.G. Amin, Optimum performance boundaries of OSTBC based AF-MIMO relay system with energy harvesting receiver. *IEEE Trans. Signal Process.* **61**(17), 4199–4213 (2013)
56. K. Long, A.V. Vasilakos, Z. Zhang, X. Chai, L. Hanzo, Full duplex techniques for 5G networks: self-interference cancellation, protocol design, and relay selection. *IEEE Commun. Mag.* **53**(5), 128–137 (2015)
57. R. Wichman, K. Pajukoski, E. Lahetkangas, R. Pitaval, O. Tirkkonen, E. Tirola, Full-duplex self-backhauling for small-cell 5G networks. *IEEE Wirel. Commun.* **22**(5), 83–89 (2015)
58. H.A. Suraweera, I. Krikidis, G. Zheng, C. Yuen, P.J. Smith, Low-complexity end-to-end performance optimization in MIMO full-duplex relay systems. *IEEE Trans. Wirel. Commun.* **13**(2), 913–927 (2014)

59. A.A. Nasir, X. Zhou, S. Durrani, R.A. Kennedy, Relaying protocols for wireless energy harvesting and information processing. *IEEE Trans. Wirel. Commun.* **12**(7), 3622–3636 (2013)
60. H. Ahmadi, S. Narayanan, M.F. Flanagan, Simultaneous uplink/downlink transmission using full-duplex single-RF MIMO. *IEEE Wirel. Commun. Lett.* **5**(1), 88–91 (2016)
61. C. Psomas, M. Mohammadi, I. Krikidis, H.A. Suraweera, Impact of directionality on interference mitigation in full-duplex cellular networks. *IEEE Trans. Wirel. Commun.* **16**(1), 1536–1276 (2017)
62. S. Goyal, P. Liu, S.S. Panwar, R.A. DiFazio, R. Yang, E. Bala, Full duplex cellular systems: will doubling interference prevent doubling capacity? *IEEE Commun. Mag.* **53**(5), 121–127 (2015)
63. S. Kashyap, E. Björnson, E.G. Larsson, On the feasibility of wireless energy transfer using massive antenna arrays. *IEEE Trans. Wirel. Commun.* **15**(5), 3466–3480 (2016)
64. K.M. Thilina, H. Tabassum, E. Hossain, D.I. Kim, Medium access control design for full duplex wireless systems: challenges and approaches. *IEEE Commun. Mag.* **53**(5), 112–120 (2015)

<http://www.springer.com/978-3-319-56668-9>

Wireless Information and Power Transfer: A New
Paradigm for Green Communications

Jayakody, D.N.K.; Thompson, J.; Chatzinotas, S.; Durrani,
S. (Eds.)

2018, XXXI, 361 p. 143 illus., 111 illus. in color.,

Hardcover

ISBN: 978-3-319-56668-9